Channel Characterization of RIS-Aided Systems Over Nakagami-m Fading Channels: A More Efficient Exact Approach

Fernando Darío Almeida García, *Member, IEEE*, Flavio du Pin Calmon, *Member, IEEE*, and José Cândido Silveira Santos Filho, *Member, IEEE*

***Abstract*—This study focuses on characterizing the channel of a reconfigurable intelligent surface (RIS)-assisted wireless system operating over Nakagami-m fading channels. Although numerous works have proposed approximate or asymptotic solutions for the RIS channel statistics (namely, the probability density function (PDF) and the cumulative distribution function (CDF)), only a limited number of studies have tackled this problem by resorting to exact approaches. Regrettably, as the number of RIS elements increases, these approaches lead to solutions that are computationally expensive or entail a high mathematical intricacy. This has prompted the analytical development undertaken in this work. Herein, our emphasis is on an exact approach. Specifically, we furnish handy and tractable formulas for the PDF and the CDF of the investigated RIS channel. The expressions introduced in this study stand out as new contributions to the literature and are arguably the most efficient *exact* solutions available to date. Numerical simulations revealed the heightened efficiency of our proposed PDF and CDF expressions against the state-of-the-art solutions. Furthermore, we conducted a performance assessment analysis for the considered RIS-assisted wireless communication system by deriving exact and asymptotic expressions for key performance indicators, namely the outage probability (OP) and the average bit-error rate (ABER). Comprehensive numerical simulations validated the accuracy of our analytical results.**

***Index Terms*—Average bit-error rate, channel characterization, cumulative distribution function, Nakagami-m fading channels, outage probability, probability density function, reconfigurable intelligent surface.**

I. Introduction

RECONFIGURABLE intelligent surfaces (RISs) have emerged as a compelling technology for upcoming wireless systems. Their capacity to intelligently reshape the wireless communication environment promises enhanced reception reliability at a cost-effective scale, positioning them as a key candidate for next-generation wireless solutions [1]. By dynamically manipulating the propagation environment, RIS can extend the coverage and range of wireless communication systems. That can be particularly beneficial in millimeter-wave communication scenarios, where signal propagation encounters significant limitations [2]. RIS can further enhance energy-efficient communication systems by optimizing signal paths and diminishing the requirement for high-powered transmissions [3]. The integration of RIS in wireless networks holds great potential for maximizing spectral efficiency and addressing the increasing demands for data transmission in a more intelligent and sustainable manner [4]. RIS has demonstrated its effectiveness in synergy with other enabling technologies, such as non-orthogonal multiple access (NOMA) and multiple-input multiple-output (MIMO) systems [5]–[7]. RIS has also found extensive application in different communication scenarios, including unmanned aerial vehicle (UAV), device-to-device (D2D), and terahertz (THz) communications [8]–[20].

Owing to the promising features and benefits of RIS, there is a shared interest in understanding its impact on wireless communication systems. Numerous research endeavors have been dedicated to analyzing the performance of wireless networks assisted by a RIS. However, to effectively asses system performance, it is first required to characterize the RIS channel. Several attempts have been carried out to characterize the RIS channel under the assumption or disregard of optimal phase shifting (OPS).[1,2] In any case, characterizing the RIS channel is a quite cumbersome task—especially for the RIS-OPS case. In the RIS-nOPS case, the channel is constructed by the sum of random vectors. Conversely, in the RIS-OPS case, the channel is formed by the sum of the product of two random variables (RVs), each RV denoting the fading channel that the signal traverses.

A. Related Works

Researchers have undertaken various efforts to assess the effectiveness of RIS technology in enhancing communication performance across diverse enabling technologies, as well as through several fading channels. Nonetheless, due to the complex mathematics involved, most of the available performance studies resort to approximate or asymptotic approaches to unveil the RIS channel statistics (namely, the probability density function (PDF) and the cumulative distribution function (CDF)). Some of these approaches include the Central Limit Theorem (CLT), the moment-matching method, Laguerre expansions, Laplace transform (LT) expansions, and the saddle-

F. D. A. García and F. P. Calmon are with the John A. Paulson School of Engineering and Applied Sciences, Harvard University, Cambridge, MA 02138, USA (email: falmeida@seas.harvard.edu; flavio@seas.harvard.edu).

J. C. S. Santos Filho is with the Wireless Technology Laboratory, Department of Communications, School of Electrical and Computer Engineering, State University of Campinas, 13083-852, Campinas, SP, Brazil (e-mail: candido@decom.fee.unicamp.br).

The work of Fernando Darío Almeida García was supported by the São Paulo Research Foundation (FAPESP) under Grant 2022/13901-5.

[1]OPS implementation requires channel state information (CSI). In practice, acquiring CSI typically involves multiple pilot transmissions [1].

[2]Hereinafter, we will refer to as "RIS-OPS" when considering a RIS with OPS, as "RIS-nOPS" when referring to a RIS with no OPS, and simply as "RIS" when referring to both (with and without OPS).

TABLE I
RIS CHANNEL STATISTICS OF PREVIOUS RIS-RELATED STUDIES

Paper	S–RIS Link	RIS–D Link	Direct Link	OPS	Method	Approach
[21]	Rayleigh	Rayleigh	No	No	CLT	Approximated
[22], [23]	Rayleigh	Rayleigh	No	Yes	CLT	Approximated
[24]	Rayleigh	Rayleigh	No	Both	CLT and Kluyver's Integral	Approx. and Exact
[7]	Rayleigh	Rayleigh	No	Both	CLT	Approx. and Bounds
[25]	Rayleigh	Rayleigh	No	No	Multivar. Fox H-function	Exact (Numerical)
[5], [26], [27]	Rayleigh	Rayleigh	No	No	Gamma	Approximated
[6], [28], [29]	Rayleigh	Rayleigh	No	Yes	Gamma	Approximated
[30]	Rayleigh	Rayleigh	No	Yes	Gamma	Approximated
[31]	Rayleigh	Rayleigh	No	Yes	Laguerre Expansion	Approximated
[32]	Rayleigh	Rayleigh	No	Yes	CLT and K_G	Approximated
[33]	Rayleigh	Rayleigh	No	No	Upper bounds	Bounds
[34]	Rayleigh	Rayleigh	Rayleigh	Yes	CLT	Approximated
[35]	Rayleigh	Rayleigh	Rayleigh	Yes	CLT	Approximated
[36]	Rayleigh	Rayleigh	Rayleigh	Yes	Saddle-Point and Chernoff Bounds	Approx. and Bounds
[37]	Rayleigh	Rayleigh	Rayleigh	No	Gamma	Approximated
[38]	Rayleigh	Rayleigh	Rayleigh	Both	Gamma	Approximated
[39]	Rayleigh	Rayleigh	No	Yes	K_G	Approximated
[40]	Rayleigh	Rician	No	Yes	K_G	Approximated
[41]	Rician	Rayleigh	No	No	Nakagami-m	Approximated
[8]	Rician	Rayleigh	No	Yes	MG	Approximated
[42]	Rician	Rician	No	Yes	Laguerre Expansion	Approximated
[43]	Rician	Rician	Rayleigh	Yes	CLT	Approximated
[44]	Rician	Rician	Rician	Yes	Gamma	Approximated
[45]	Rician	Rician	K_G	No	Nakagami-m	Approximated
[20]	MG	MG	No	Yes	MG	Approximated
[46]	MG	MG	No	Yes	MG	Approximated
[10], [15], [47]	Nakagami-m	Nakagami-m	No	No	Gamma	Approximated
[48], [49]	Nakagami-m	Nakagami-m	No	No	CLT	Approximated
[16]	Nakagami-m	Nakagami-m	No	Yes	LT	Approximated
[17]	Nakagami-m	Nakagami-m	No	Yes	LT and CLT	Approximated
[50]	Nakagami-m	Nakagami-m	No	No	HT	Exact
[11], [51]	Nakagami-m	Nakagami-m	No	Yes	Gamma	Approximated
[52]	Nakagami-m	Nakagami-m	No	Yes	CLT	Approximated
[53]	Nakagami-m	Nakagami-m	No	Yes	Laguerre Expansion	Approximated
[54]	Nakagami-m	Nakagami-m	Rayleigh	Yes	CLT	Approximated
[14]	Nakagami-m	Nakagami-m	Nakagami-m	Yes	Laguerre Expansion	Approximated
[55]	Nakagami-m	Nakagami-m	Nakagami-m	Yes	Gamma	Approximated
[12]	Nakagami-m	Nakagami-m	Nakagami-m	Both	CLT and Gamma	Approximated
[9], [56]	Nakagami-m	Nakagami-m	Nakagami-m	Yes	Gamma	Approximated
[13], [57]	Nakagami-m	Nakagami-m	Nakagami-m	Yes	CLT	Approximated
[58]	Nakagami-m	Nakagami-m	Nakagami-m	No	Hankel Transform	Exact
[59]	Nakagami-m	Nakagami-m	Nakagami-m	Yes	Gamma and Log-Normal	Approximated
[60]	Nakagami-m	Nakagami-m	Nakagami-m	Yes	CLT and Gil-Pelaez's Integral	Approximated
[61]	Nakagami-m	Nakagami-m	Nakagami-m	Both	CLT, HT, and Gil-Pelaez's Integral	Approx. and Exact (Numerical)
[62]	Rician/Nakagami-m	Rician/Nakagami-m	No	Yes	CLT and Gamma	Approximated
[63]	Nakagami-m/α-μ /Rician/K_G/FS-$\mathcal{F}$	Nakagami-m/α-μ /Rician/K_G/FS-$\mathcal{F}$	No	Both	Multivar. Fox H-function	Exact (Numerical)
[18]	FTR	FTR	No	Yes	Multivar. Fox H-function	Exact (Numerical)
[64]	DGG	DGG	DGG	Yes	Multivar. Fox H-function	Exact (Numerical)
[65]	Weibull	Weibull	Rayleigh	No	Gamma	Approximated
[19]	α-μ	α-μ	No	Both	CLT and Gamma	Approximated
[66], [67]	κ-μ	κ-μ	κ-μ	Yes	Gamma	Approximated
[68]	κ-μ	κ-μ	κ-μ	No	Gamma and KL Diverg.	Approximated
[69]	Extended η-μ	Extended η-μ	Extended η-μ	Yes	Gil-Pelaez's Integral	Exact (Numerical)

point approximation. On the other hand, a limited number of works rely on exact approaches to acquire the RIS channel statistics. These approaches include the multivariate Fox H-function, the Gil-Pealez's integral, the Kluyver's integral, and the Hankel transform (HT). Table I compiles the RIS channel statistics of previous representative studies. More precisely, Table I outlines: the fading model between the source and the RIS (second column); the fading model between the RIS and the destination (third column); the presence or absence of the direct channel (fourth column); the assumption or disregard of OPS (fifth column); the method applied to characterize the RIS channel (e.g., CLT, moment-matching method, and saddle-point) (sixth column); and the nature of the solution (e.g., bounds, asymptotic, approximated, exact) (seventh column).

B. Drawbacks and Limitations

While the reported approximate and asymptotic solutions can rapidly and efficiently compute the RIS channel statistics, they encounter inherent accuracy and convergence challenges. For instance, the CLT provides a good approximation for the

"central" (near the peak) region of the distribution. However, the CLT lacks accuracy in estimating tail probabilities—both left and right tails—, making it less effective in capturing rare events probabilities, particularly for distributions with heavy tails. Additionally, the sample size (i.e., the number of RVs) should be sufficiently large for the CLT to be applied. It is worth noting that convergence to a normal distribution may be slower, especially if the underlying distributions deviate significantly from normality. Several other studies utilize the moment-matching method to approximate the PDF of the RIS channel to a Gamma, Nakagami-m, generalized-K (K_G), or Log-normal distribution. Nonetheless, the moment-matching method may not be accurate in approximating right-tail probabilities. That is primarily because the moment-matching method focuses on matching lower-order moments, and when dealing with heavy-tailed distributions—higher-order moments play a crucial role in characterizing the tail distributions—, ignoring these higher moments can result in inaccuracies at the extreme values of the distribution. Bounds and asymptotic approximations (e.g., saddle-point approximation), on the other hand, are deemed effective for approximating tail distributions in scenarios where the CLT or the moment-matching method may lack accuracy. However, their utility lies in approximating the PDF within a specific region, not encompassing the entire PDF, a crucial aspect in certain wireless scenarios.

To overcome the aforementioned issues, some studies have resorted to numerical approaches (e.g., multivariate Fox H-function, Gil-Pealez's integral, Kluyver's integral) to provide exact solutions for the RIS channel statistics. Regrettably, these solutions are either computationally expensive or involve significant mathematical complexity. Furthermore, due to their purely numerical nature, their accuracy is restricted by machine precision.

C. Motivation and Contributions

Despite the high reliability of exact solutions, only a few works address this problem in an exact manner. However, as stated earlier, these solutions are computationally expensive or entail a high mathematical intricacy. This has motivated the analytical development pursued in this study. This paper endeavors to derive new exact and efficient formulas for the RIS-OPS channel statistics. Our ultimate goal is to accurately and efficiently assess the performance of a wireless communication system assisted by a RIS-OPS and subject to Nakagami-m fading channels. The main contributions of this work are as follows.

1) We propose novel tractable and efficient formulas for the *exact* statistics (PDF and CDF) of the RIS-OPS channel. To do so, we assume independent and identically distributed (i.i.d.) Nakagami-m fading channels. Our derived formulations are deemed to be new in the literature and are arguably the most efficient exact solutions reported to date.
2) We carry out a performance assessment analysis for a wireless communication system assisted by a RIS-OPS. Concretely, we obtain exact and asymptotic expressions for the key performance indicators (KPIs) of the system, specifically the outage probability (OP) and the average bit-error rate (ABER).
3) We conduct an efficiency analysis comparing our proposed PDF and CDF expressions with the existing state-of-the-art solutions. Numerical simulations demonstrate that our expressions outperform the competing exact solutions in terms of accuracy, tractability, and computation time.[3]

D. Structure and Notation

The remainder of this paper is structured as follows. In Section II, we introduce the RIS-aided wireless system model. In Section III, we propose new exact formulas for the RIS channel statistics. In Section IV, we assess the performance of the investigated wireless communication system assisted by RIS-OPS. In Section V, we corroborate our analytical findings through numerical simulations. Finally, in Section VI, we summarize and conclude this paper.

In the sequel, $\mathbb{E}[\cdot]$, denotes expectation; $\Pr[\cdot]$, probability; $(\cdot)^T$, transpose; $(\cdot)^H$, Hermitian transpose; $\mathrm{diag}[\cdot]$, returns the diagonal elements of a square matrix; $\mathbf{Re}[\cdot]$, returns the real part of a complex number; $\min(\cdot,\cdot)$ and $\max(\cdot,\cdot)$, are the minimum and maximum operators, respectively; $|\cdot|$, denotes absolute value; $\lfloor\cdot\rfloor$ and $\lceil\cdot\rceil$ are the floor and ceiling operators, respectively; $\max_n\{\cdot\}$, denotes the maximum value of a set of n elements; $\sup_n\{\cdot\}$, denotes the supremum of a set of n elements; $\Gamma(\cdot)$, the gamma function [70, eq. 6.1.1]; $\Upsilon(\cdot,\cdot)$, the lower incomplete gamma function [71, eq. (8.2.1)]; $\Gamma(\cdot,\cdot)$, the upper incomplete gamma function [72, eq. (8.350.2)]; $K_\nu(\cdot)$, the modified Bessel function of the second kind and νth order [73, eq. (03.04.02.0001.01)]; ${}_2F_2(\cdot,\cdot;\cdot,\cdot;\cdot)$, the generalized hypergeometric function [73, eq. (07.25.02.0001.01)]; $\mathcal{CN}(\mu,\sigma^2)$, stands for a complex Gaussian distribution with mean μ and variance σ^2; $\mathcal{NK}(m,\Omega)$, signifies a Nakagami-m distribution with shape parameter m and spread parameter Ω; $\sim$, denotes "distributed as"; $\mathrm{i}=\sqrt{-1}$, the imaginary unit; $\mathbb{C}$, the set of complex numbers; $\mathbb{R}$, the set of real numbers; $\mathbb{R}^+$, the set of positive real numbers excluding zero; $\mathbb{N}$, the set of natural numbers; $\mathbb{Z}$, the set of integer numbers; and $\simeq$, "asymptotically equal to around zero," i.e., $h(x)\simeq g(x) \iff \lim_{x\to 0}\frac{h(x)}{g(x)}=1$.

II. System Model

Herein, we consider that a RIS composed of L elements assists the communication between a source node (S) and a destination node (D). Both nodes are equipped with a single antenna and operate in half-duplex mode. We also consider that the direct link between the source and destination nodes is blocked due to the presence of big obstacles, such as buildings and/or trees, as illustrated in Fig. 1.

Let $\mathbf{h}_1 = [\tilde{h}_{1,1},\ldots,\tilde{h}_{1,L}]^T \in \mathbb{C}^{L\times 1}$ and $\mathbf{h}_2 = [\tilde{h}_{2,1},\ldots,\tilde{h}_{2,L}]^T \in \mathbb{C}^{L\times 1}$ be the vectors containing the channel coefficients between S and the ℓth element of the RIS

[3]Computation time or elapsed time refers to the actual amount of time it takes for a computer or system to perform a specific computational task, from the initiation to the completion.

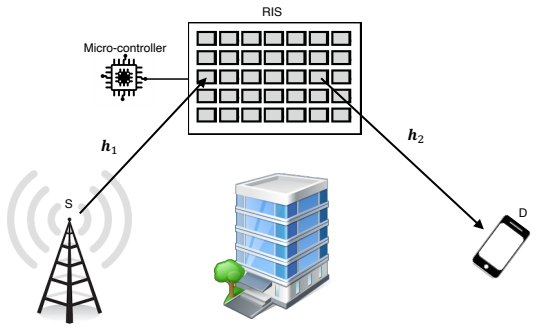

Fig. 1. System model.

($\ell = 1, 2, \ldots, L$), and between the ℓth element of the RIS and D, respectively, where $\tilde{h}_{r,\ell} = h_{r,\ell} e^{\mathrm{i}\,\phi_{r,\ell}}$ ($r \in \{1, 2\}$) with $h_{r,\ell}$ and $\phi_{r,\ell}$ being the envelope and phase components of the channel coefficient, respectively. Additionally, we assume that $\{h_{1,\ell}\}_{\ell=1}^{L}$ and $\{h_{2,\ell}\}_{\ell=1}^{L}$ are sets of i.i.d. Nakagami-m RVs with $h_{1,\ell} \sim \mathcal{NK}(m_1, \Omega_1)$ and $h_{2,\ell} \sim \mathcal{NK}(m_2, \Omega_2)$.[4] Accordingly, the received signal at D is given by

$$y = \sqrt{P}\,(d_1 d_2)^{-u/2} \left(\mathbf{h}_1^H \Theta \mathbf{h}_2\right) s + w, \tag{1}$$

where P is the transmitted power, d_1 and d_2 are the distances of the S-RIS and RIS-D links, respectively, u is the path loss exponent, s is the transmitted data symbol satisfying (without loss of generality) $\mathbb{E}[|s|^2] = 1$, $w \sim \mathcal{CN}(0, 2\sigma^2)$ is the complex additive white Gaussian noise (AWGN), and $\Theta = \mathrm{diag}\left[e^{\mathrm{i}\,\theta_1}, \ldots, e^{\mathrm{i}\,\theta_L}\right]$ is the RIS reflection matrix with $\theta_\ell \in [0, 2\pi]$ denoting the associated ℓth phase shift.

From (1), the instantaneous signal-to-noise ratio (SNR) at D can be written as

$$\begin{aligned}\gamma =& \rho \left|\left(\mathbf{h}_1^H \Theta \mathbf{h}_2\right)\right|^2 \\ =& \rho \left|\sum_{\ell=1}^{L} h_{1,\ell} h_{2,\ell} e^{\mathrm{i}(\theta_\ell + \phi_{1,\ell} + \phi_{2,\ell})}\right|^2,\end{aligned} \tag{2}$$

where $\rho = P\,(d_1 d_2)^{-u}/2\sigma^2$ is the average SNR per symbol.

Aiming at maximizing the instantaneous SNR, we assume that the RIS has a perfect knowledge of the CSI. Therefore, OPS can be applied (i.e., $\theta_\ell = -\phi_{1,\ell} - \phi_{2,\ell}$) and the instantaneous SNR at D reduces to

$$\gamma = \rho \left|\sum_{\ell=1}^{L} h_{1,\ell} h_{2,\ell}\right|^2. \tag{3}$$

In order to unveil the system performance of the considered RIS-aided wireless system, it is imperative to characterize the instantaneous SNR γ in (3), which involves finding the sum statistics of the product of two Nakagami-m RVs. Although, there are several works that address this problem via approximate or asymptotic procedures, only a few works address this problem in an exact manner. Unfortunately, the available exact approaches carry some computational limitations. This has spurred the analytical development pursued in this study.

In the next section, we will introduce new exact and efficient formulas for the sum statistics required in (3).

[4]The Nakagami-m fading model is a generic and versatile distribution that includes, as special case, the Rayleigh distribution (typically used for non-line-of-sight scenarios). In addition, it can also closely approximate the Hoyt and Rice distributions [9], [54].

III. Required Sum Statistics

Let us define H as the sum of i.i.d. RVs, namely

$$H \triangleq \sum_{\ell=1}^{L} H_\ell, \tag{4}$$

where $H_\ell = h_{1,\ell} h_{2,\ell}$ is the product of two Nakagami-m RVs $h_{1,\ell}$ and $h_{2,\ell}$, each having a PDF given by

$$f_{h_{r,\ell}}(h_{r,\ell}) = \frac{2\left(\frac{m_r}{\Omega_r}\right)^{m_r} h_{r,\ell}^{2m_r - 1}}{\Gamma(m_r)} \exp\left(-\frac{m_r h_{r,\ell}^2}{\Omega_r}\right), \tag{5}$$

where m_r and Ω_r ($r \in \{1, 2\}$) are their corresponding shape and spread parameters, respectively.

The PDF of H_ℓ is given by [74, eq. (6)]

$$f_{H_\ell}(h_\ell) = \frac{4\psi^{\frac{1}{2}(m_1+m_2)} h_\ell^{m_1+m_2-1}}{\Gamma(m_1)\,\Gamma(m_2)} K_{m_1 - m_2}\left(2\sqrt{\psi} h_\ell\right), \tag{6}$$

where $\psi = \left(\frac{m_1 m_2}{\Omega_1 \Omega_2}\right)$.

In the following two theorems, we derive the *exact* statistics for the sum outlined in (4).

Theorem 1. *The PDF and the CDF for the sum in* (4) *when* $|m_1 - m_2| \in \mathbb{R}^+ \setminus \mathscr{A}$*, with* $\mathscr{A} = \mathbb{N} - \frac{1}{2}$*, are respectively given by*

$$\begin{aligned} f_H(h) =& \alpha^L h^{-1} \exp\left(-2h\sqrt{\psi}\right) \\ &\times \sum_{i=0}^{\infty} \frac{\delta_i\, 2^i \left(h\sqrt{\psi}\right)^{2L\min(m_1, m_2) + i}}{\Gamma\left(i + 2L\min(m_1, m_2)\right)} \end{aligned} \tag{7}$$

$$\begin{aligned} F_H(h) =& \alpha^L 4^{-L\min(m_1, m_2)} \\ &\times \sum_{i=0}^{\infty} \frac{\Upsilon\left(2L\min(m_1, m_2) + i, 2h\sqrt{\psi}\right)}{\Gamma\left(i + 2L\min(m_1, m_2)\right)}, \end{aligned} \tag{8}$$

where

$$\alpha = \frac{\sqrt{\pi} 4^{1 - |m_1 - m_2|} \Gamma\left(2|m_1 - m_2|\right)}{\Gamma(m_1)\,\Gamma(m_2)\,\Gamma\left(\frac{1}{2} - |m_1 - m_2|\right)}, \tag{9}$$

and the coefficients δ_i *(*$i \geq 0$*) are given by*

$$\delta_0 = \left[\frac{\Gamma\left(\frac{1}{2} - |m_1 - m_2|\right)\Gamma\left(2\min(m_1, m_2)\right)}{\Gamma\left(|m_1 - m_2| + \frac{1}{2}\right)}\right]^L \tag{10a}$$

$$\begin{aligned} \delta_i =& \frac{1}{i\delta_0^{1/L}} \sum_{k=1}^{i} \theta_k \delta_{i-k}\left(kL + k - i\right) \\ &\times (-2)^k \Gamma\left(k + 2\min(m_1, m_2)\right), \qquad i \geq 1. \end{aligned} \tag{10b}$$

Additionally, θ_k *in* (10b) *can be obtained as*

$$\theta_k = \frac{1}{k!} \sum_{j=k}^{\infty} \binom{j-1}{k-1} \frac{\Gamma\left(j - |m_1 - m_2| + \frac{1}{2}\right)}{\Gamma\left(j + |m_1 - m_2| + \frac{1}{2}\right)}. \tag{11}$$

Proof. Please, see Appendix A. ■

In Appendix C, we demonstrate that the sum PDF in (7) converges uniformly and absolutely on h. A similar approach to that used in Appendix C can be applied to establish the uniform and absolute convergence of the sum CDF in (8).

Below, we provide some computational remarks concerning the PDF and CDF expressions outlined in Theorem 1.

Computational Remark 1: There are three key distinctions between the derived PDF and CDF expressions provided in Theorem 1 and the current competing exact solutions given in [61] and [63]: (i) accuracy, (ii) computational burden, and (iii) mathematical tractability.

(i) Accuracy: As seen in Table I, the state-of-the-art solutions for computing the RIS-OPS channel statistics under i.i.d. Nakagami-m fading channels are given in [61] and [63]. These solutions rely on the Gil-Pelaez's integral and the multivariate Fox H-function. Unfortunately, although these approaches are exact in a mathematical sense, they are limited by machine precision due to their purely numerical nature. More precisely, both the Gil-Pelaez and the multivariate Fox H-function approaches rely on the *numerical* evaluation of infinite-range integrals—one integral for the Gil-Pelaez approach and multiple complex integrals for the multivariate Fox H-function. Consequently, an accuracy control cannot be assured since it depends entirely on the software's numerical integration method (e.g., trapezoidal rule, Riemann rule, quasi Monte Carlo) and the initial parameter settings (e.g., accuracy goal, working precision, maximum number of evaluation points). For instance, a target accuracy of 10^{-20} can be challenging to attain—if not impossible. In contrast, (7) and (8) can reach any target accuracy by merely increasing the number of terms in their sums, albeit at the expense of additional computational load. In particular, by fixing the number of terms to 200 and 20 in (7) and (11), respectively, yields an outstanding PDF accuracy of less than 10^{-20}. This aspect will be addressed in detail in Section V.

(ii) Computational Burden: The numerical evaluation of Gil-Pelaez's integral poses challenges due to the oscillatory and slowly decaying behavior of the integrand, leading to the addition of a substantial number of regions with nearly equal magnitudes and alternating signs, contributing to an increase in the computation time of the integration routine. On the other hand, the computational burden of the multivariate Fox H-function approach rises in tandem with the number of RIS elements (L). Indeed, in order to compute the RIS-OPS channel statistics, one must execute multiple infinite-range complex integrations, where the number of complex integrals equals the number of RIS elements—this holds true even for the i.i.d. case—, thereby escalating its computational burden and possibly leading to instability issues. In contrast, (7) and (8) require only addition and multiplication operations and do not involve any numerical integration. Moreover, the computational burden of (7) and (8) remains unchanged as no additional infinite (or finite) summations or products are incorporated in the computation when the number of RIS elements grows. More importantly, as (7) and (8) are expressed in terms of elementary functions (e.g., gamma and exponential functions), they can be efficiently computed in any mathematical software. In particular, for a RIS-OPS scenario with i.i.d. Nakagami-m fading channels, (7) and (8) proved faster than the solutions in [61] and [63]. This aspect will be thoroughly confirmed in Section V.

(iii) Mathematical Tractability: It should be noted that the mathematical intricacy of the solutions provided in [61] and [63] escalates with L. For instance, the number of Gauss hypergeometric functions in the integration kernel of [61] increases with the growth of L. Similarly, the number of gamma functions in the integration kernel of [63] grows along with L. Conversely, the number of gamma functions as well as other mathematical functions in (7) and (8) remains constant as L grows, thus retaining its mathematical complexity. Mathematical tractability is a crucial feature when deriving the KPIs of any communication system. Specifically, it will allow us to evaluate them in an efficient or closed-form manner, as will be seen in Section IV.

A. Truncation Error Analysis

When the number of terms in (7) and (8) is fixed to t, we can respectively defined the associated truncation errors as

$$\begin{aligned}\epsilon_{f_H}(h) \triangleq& \alpha^L h^{-1} \exp\left(-2h\sqrt{\psi}\right) \\ &\times \sum_{i=t}^{\infty} \frac{\delta_i\, 2^i \left(h\sqrt{\psi}\right)^{2L\min(m_1,m_2)+i}}{\Gamma\left(i+2L\min\left(m_1,m_2\right)\right)} \end{aligned} \tag{12}$$

$$\begin{aligned}\epsilon_{F_H}(h) \triangleq& \alpha^L 4^{-L\min(m_1,m_2)} \\ &\times \sum_{i=t}^{\infty} \frac{\delta_i \Upsilon\left(2L\min\left(m_1,m_2\right)+i, 2h\sqrt{\psi}\right)}{\Gamma\left(2L\min\left(m_1,m_2\right)+i\right)}. \end{aligned} \tag{13}$$

In Appendix D, we show that (12) can be upper bounded in closed form as

$$\begin{aligned}\epsilon_{f_H}(h) <& \sqrt{\psi}\alpha^L 2^{1-2L\min(m_1,m_2)} \\ &\times \frac{\Upsilon\left(2L\min\left(m_1,m_2\right)+t-1, 2h\sqrt{\psi}\right)}{\Gamma\left(2L\min\left(m_1,m_2\right)+t-1\right)}. \end{aligned} \tag{14}$$

In like manner, in Appendix E, we demonstrate that (13) can be upper bounded in closed form as

$$\begin{aligned}\epsilon_{F_H}(h) <& \alpha^L 4^{-L\min(m_1,m_2)} \left(2h\sqrt{\psi}\right)^{2L\min(m_1,m_2)} \\ &\times \Bigg[\frac{\left(2h\sqrt{\psi}\right)^t}{\Gamma\left(t+2L\min\left(m_1,m_2\right)+1\right)} \\ &+ \exp\left(2h\sqrt{\psi}\right)\left(4h^2\psi\right)^{-L\min(m_1,m_2)} \\ &\times \frac{\Upsilon\left(2L\min\left(m_1,m_2\right)+t+1, 2h\sqrt{\psi}\right)}{\Gamma\left(2L\min\left(m_1,m_2\right)+t+1\right)}\Bigg]. \end{aligned} \tag{15}$$

Since $\lim\limits_{t\to\infty} \frac{b^t}{\Gamma(a+t)} = 0$ and $\lim\limits_{t\to\infty} \frac{\Upsilon(a+t,h)}{\Gamma(a+t)} = 0$ for $a, b \in \mathbb{R}$, it is evident that (14) and (15) approach to zero as the number of terms t increases.

The expressions (14) and (15) hold practical significance for analyzing the accuracy of the PDF and CDF expressions given in Theorem 1. More precisely, they provide the *sufficient* number of terms in (7) and (8) to achieve a desired accuracy.

In the following theorem, we alleviate the PDF-parameter constraint prevalent in Theorem 1. Specifically, we provide closed-form expressions for sum statistics in (4) taking into account $|m_1 - m_2| \in \mathbb{N} - \frac{1}{2}$.

Theorem 2. *The PDF and the CDF for the sum in* (4) *when* $|m_1 - m_2| \in \mathscr{A}$*, with* $\mathscr{A} = \mathbb{N} - \frac{1}{2}$*, are respectively given in closed form as*

$$f_H(h) = \beta^L \exp\left(-2h\sqrt{\psi}\right) \sum_{i=0}^{Lm^\dagger} \frac{\varphi_i \, h^{2L\min(m_1,m_2)+i-1}}{\Gamma\left(i + 2L\min\left(m_1, m_2\right)\right)} \tag{16}$$

$$F_H(h) = \beta^L \sum_{i=0}^{Lm^\dagger} \frac{\varphi_i \left(2\sqrt{\psi}\right)^{-i-2L\min(m_1,m_2)}}{\Gamma\left(i + 2L\min\left(m_1, m_2\right)\right)} \times \Upsilon\left(i + 2L\min\left(m_1, m_2\right), 2h\sqrt{\psi}\right), \tag{17}$$

where $m^\dagger = \left\lfloor |m_1 - m_2| - \frac{1}{2} \right\rfloor$,

$$\beta = \frac{2^{1-2m^\dagger}\sqrt{\pi}\sqrt{\psi}^{m_1+m_2-m^\dagger-\frac{1}{2}}}{\Gamma\left(m_1\right)\Gamma\left(m_2\right)}, \tag{18}$$

and the coefficients φ_i $(i \geq 0)$ *are given by*

$$\varphi_0 = \left[\frac{\Gamma\left(2\min\left(m_1, m_2\right)\right)\Gamma\left(|m_1 - m_2| + m^\dagger + \frac{1}{2}\right)}{\Gamma\left(m^\dagger + 1\right)\Gamma\left(m^\ddagger + |m_1 - m_2| + \frac{1}{2}\right)}\right]^L \tag{19a}$$

$$\varphi_i = \frac{1}{i\phi_0} \sum_{j=1}^{i} \phi_j \varphi_{i-j} \left(Lj + j - i\right) \left(4\sqrt{\psi}\right)^j \times \Gamma\left(2\min\left(m_1, m_2\right) + j\right), \qquad 1 \leq i \leq m^\dagger \tag{19b}$$

$$\varphi_i = \frac{1}{i\phi_0} \sum_{j=1}^{m^\dagger} \phi_j \varphi_{i-j} \left(Lj + j - i\right) \left(4\sqrt{\psi}\right)^j \times \Gamma\left(2\min\left(m_1, m_2\right) + j\right), \qquad m^\dagger + 1 \leq i \leq Lm^\dagger. \tag{19c}$$

Moreover, $m^\ddagger = \left\lceil \frac{1}{2} - |m_1 - m_2| \right\rceil$ *and* ϕ_j *in* (19c) *can be calculated as*

$$\phi_j = \frac{\Gamma\left(-j + |m_1 - m_2| + m^\dagger + \frac{1}{2}\right)}{\Gamma\left(-j + m^\dagger + 1\right)\Gamma\left(j + |m_1 - m_2| + m^\ddagger + \frac{1}{2}\right)}.$$

Proof. Please, see Appendix F. ∎

Computational Remark 2: Since (16) and (17) are given in closed form, they attain constant runtimes and are exempt from accuracy limitations.

It is worth emphasizing that the PDF and CDF expressions provided in Theorem 1 and Theorem 2 are the main contributions of this work and are arguably the most efficient solutions reported to date for the investigated scenario.

IV. Performance Evaluation

In this section, we assess the performance of the wireless communication system detailed in Section II. More precisely, we derive exact and asymptotic formulas for the KPIs, namely OP and ABER. In the sequel, we will divide the analysis for each KPI into two cases. We will refer as Case I when adopting $|m_1 - m_2| \in \mathbb{R}^+ \setminus \mathscr{A}$, and as Case II when adopting $|m_1 - m_2| \in \mathscr{A}$.

A. Outage Probability

The OP is defined as the probability that the instantaneous SNR falls below a pre-determined threshold γ_{th}, that is,

$$P_{\text{out}} \triangleq \Pr\left[\gamma \leq \gamma_{\text{th}}\right]. \tag{20}$$

From (3), the OP can be computed in terms of the CDF of H as

$$P_{\text{out}} = \Pr\left[\rho H^2 \leq \gamma_{\text{th}}\right] = F_H\left(\sqrt{\frac{\gamma_{\text{th}}}{\rho}}\right). \tag{21}$$

1) Case I: From (8), an exact OP expression can be readily derived as

$$P_{\text{out}}^{\mathbb{R}^+\setminus\mathscr{A}} = \alpha^L 4^{-L\min(m_1,m_2)} \times \sum_{i=0}^{\infty} \frac{\delta_i \Upsilon\left(2L\min\left(m_1, m_2\right) + i, 2\sqrt{\frac{L\psi\gamma_{\text{th}}}{\rho}}\right)}{\Gamma\left(2\min\left(m_1, m_2\right) + i\right)}. \tag{22}$$

Next, we provide an asymptotic analysis for the OP, which allows us to gain valuable insights into how the fading parameters affect the system performance in a high SNR regime—a regime of paramount interest in wireless communications.

Notice that in the high SNR regime (i.e., when $\rho \to \infty$), only the first term dominates the series in (22). Hence, considering only this term, we have

$$P_{\text{out}}^{\mathbb{R}^+\setminus\mathscr{A}} \simeq \delta_0 \alpha^L 4^{-L\min(m_1,m_2)} \times \frac{\Upsilon\left(2L\min\left(m_1, m_2\right), 2\sqrt{\frac{\psi\gamma_{\text{th}}}{\rho}}\right)}{\Gamma\left(2L\min\left(m_1, m_2\right)\right)}. \tag{23}$$

Now, using the series representation of the lower incomplete gamma function [70, eq. (6.5.12)] in (23), we get

$$P_{\text{out}}^{\mathbb{R}^+\setminus\mathscr{A}} \simeq \frac{\delta_0 \alpha^L 2^{-2L\min(m_1,m_2)}}{\Gamma\left(2L\min\left(m_1, m_2\right)\right)} \left(2\sqrt{\frac{\psi\gamma_{\text{th}}}{\rho}}\right)^{2L\min(m_1,m_2)} \times \sum_{k=0}^{\infty} \frac{1}{k!\left(2L\min\left(m_1, m_2\right) + k\right)} \left(-2\sqrt{\frac{\psi\gamma_{\text{th}}}{\rho}}\right)^k. \tag{24}$$

Since the first term in (24) becomes the most representative as ρ approaches infinity, we can finally obtain an asymptotic closed-form OP expression as

$$P_{\text{out}}^{\mathbb{R}^+\setminus\mathscr{A}} \simeq \left(\rho \mathcal{C}_{\text{out}}^*\right)^{-\mathcal{D}_{\text{out}}^*}, \tag{25}$$

where $\mathcal{D}_{\text{out}}^* = L\min\left(m_1, m_2\right)$ is the OP diversity gain and

$$\mathcal{C}_{\text{out}}^* = \frac{1}{\psi\gamma_{\text{th}}} \left[\frac{\delta_0 \alpha^L}{\Gamma\left(2L\min\left(m_1, m_2\right) + 1\right)}\right]^{-\frac{1}{\mathcal{D}_{\text{out}}^*}} \tag{26}$$

is the OP coding gain.

2) Case II: From (17), an exact OP expression can be easily obtained as

$$P_{\text{out}}^{\mathscr{A}} = \beta^L \sum_{i=0}^{Lm^\dagger} \frac{\varphi_i \left(2\sqrt{\psi}\right)^{-i-2L\min(m_1,m_2)}}{\Gamma\left(i+2L\min\left(m_1,m_2\right)\right)} \times \Upsilon\left(i+2L\min\left(m_1,m_2\right), 2\sqrt{\frac{\psi\gamma_{\text{th}}}{\rho}}\right). \quad (27)$$

To obtain an asymptotic expression for the OP, we employ the same procedure as in (25). That is, we focus on the first term of the series in (27) and subsequently apply the series representation of the lower incomplete gamma function. Ultimately, the asymptotic closed-form OP expression is given by

$$P_{\text{out}}^{\mathscr{A}} \simeq \left(\rho\, \mathcal{C}_{\text{out}}^{\dagger}\right)^{-\mathcal{D}_{\text{out}}^{\dagger}}, \quad (28)$$

where $\mathcal{D}_{\text{out}}^{\dagger} = L\min\left(m_1,m_2\right)$ is the OP diversity gain and

$$\mathcal{C}_{\text{out}}^{\dagger} = \frac{1}{\gamma_{\text{th}}}\left[\frac{\varphi_0 \beta^L}{\Gamma\left(2L\min\left(m_1,m_2\right)+1\right)}\right]^{-\frac{1}{\mathcal{D}_{\text{out}}^{\dagger}}} \quad (29)$$

is the OP coding gain.

B. Average Bit-Error Rate

Across various modulation formats, the ABER is given by

$$P_{\text{b}} = \frac{1}{2\Gamma(b)} \int_0^{\infty} \Gamma\left(b, d\rho h^2\right) f_H(h) \mathrm{d}h, \quad (30)$$

where b and d are modulation-dependent parameters. For instance, $b=0.5$ and $d=1$ signify coherent binary phase-shift keying (BPSK) modulation; $b=0.5$ and $d=0.5$, coherent binary frequency shift keying (BFSK) modulation; and $b=1$ and $d=1$, differential BPSK modulation.

1) Case I: An exact expression for the ABER can be obtained by plugging (7) into (30), yielding

$$P_{\text{b}}^{\mathbb{R}^+\setminus\mathscr{A}} = \frac{\alpha^L}{2\Gamma(b)} \sum_{i=0}^{\infty} \frac{\delta_i 2^i \left(\sqrt{\psi}\right)^{2L\min(m_1,m_2)+i}}{\Gamma\left(i+2L\min\left(m_1,m_2\right)\right)} \mathcal{I}_i(\rho), \quad (31)$$

where

$$\mathcal{I}_i(\rho) = \int_0^{\infty} \exp\left(-2\sqrt{\psi}h\right) h^{i+2L\min(m_1,m_2)-1} \times \Gamma\left(b, d\rho h^2\right) \mathrm{d}h. \quad (32)$$

Due to the presence of the upper incomplete gamma function in the integrand, (32) cannot be evaluated in closed form. Therefore, we apply a residue-based approach.

Replacing the upper incomplete gamma function by its contour integral representation [73, eq. (06.06.07.0005.01)] in (32), we have

$$\mathcal{I}_i(\rho) = \int_0^{\infty} \exp\left(-2\sqrt{\psi}h\right) h^{i+2L\min(m_1,m_2)-1} \times \frac{1}{2\pi\,\mathrm{i}} \oint_{\mathcal{L}_{\text{C}_1}} \frac{\Gamma(\xi)\Gamma(b+\xi)}{\Gamma(\xi+1)} \left(d\rho h^2\right)^{-\xi} \mathrm{d}\xi\, \mathrm{d}h, \quad (33)$$

where ξ is a complex variable of integration and $\mathcal{L}_{\text{C}_1}$ is a complex path parallel to the imaginary axis, starting at $(\max(-b,0) - \infty\,\mathrm{i})$ and ending at $(\max(-b,0) + \infty\,\mathrm{i})$.

Interchanging the order of integration in (33) by invoking Fubini's theorem then evaluating the inner integral,[5] we obtain

$$\mathcal{I}_i(\rho) = \frac{\left(2\sqrt{\psi}\right)^{-i-2L\min(m_1,m_2)}}{2\pi\,\mathrm{i}} \oint_{\mathcal{L}_{\text{C}_2}} \frac{\Gamma(\zeta)\Gamma(b+\zeta)}{\Gamma(\zeta+1)} \times \Gamma\left(i+2L\min\left(m_1,m_2\right)-2\zeta\right) \left(\frac{d\rho}{4\psi}\right)^{-\zeta} \mathrm{d}\zeta, \quad (34)$$

where ζ is a new complex variable of integration and $\mathcal{L}_{\text{C}_2}$ is a new complex path that appears since the integration over x deformed the previous integration path. Specifically, we choose $\mathcal{L}_{\text{C}_2}$ to be a contour that separates the poles of $\Gamma(\zeta)$ and $\Gamma(b+\zeta)$ from those of $\Gamma\left(i+2L\min\left(m_1,m_2\right)-2\zeta\right)$ in a counterclockwise sense. We adopt this contour as it prevents $\mathcal{I}_i(\rho)$ from having replicated poles and ensures the convergence of the complex integral.

At this point, the contour integral in (34) can be evaluated via residues as [76]

$$\mathcal{I}_i(\rho) = \left(2\sqrt{\psi}\right)^{-i-2L\min(m_1,m_2)} \times \sum_{j=0}^{\infty} \mathcal{R}\left[\Xi(\zeta); \zeta = \frac{1}{2}(i+j+2L\min\left(m_1,m_2\right))\right], \quad (35)$$

where $\mathcal{R}[\cdot]$ denotes the residue of the function $\Xi(\zeta)$ evaluated at the poles $\zeta = \frac{1}{2}(i+j+2L\min\left(m_1,m_2\right))$, and

$$\Xi(\zeta) = \frac{\Gamma(\zeta)\Gamma(b+\zeta)\Gamma\left(i-2\zeta+2L\min\left(m_1,m_2\right)\right)}{\Gamma(\zeta+1)} \left(\frac{d\rho}{4\psi}\right)^{-\zeta} \quad (36)$$

is the integration kernel of (34).

After computing the residues in (35), we get

$$\mathcal{I}_i(\rho) = \left(2\sqrt{\psi}\right)^{-i-2L\min(m_1,m_2)} \times \sum_{j=0}^{\infty} \frac{(-1)^j \Gamma\left(\frac{1}{2}\left(2b+i+j+2L\min\left(m_1,m_2\right)\right)\right)}{\left(i+j+2L\min\left(m_1,m_2\right)\right)\Gamma(j+1)} \times \left(2\sqrt{\frac{\psi}{d\rho}}\right)^{i+j+2L\min(m_1,m_2)}. \quad (37)$$

Replacing (37) into (31), we obtain

$$P_{\text{b}}^{\mathbb{R}^+\setminus\mathscr{A}} = \frac{\alpha^L 2^{-2L\min(m_1,m_2)-1}}{\Gamma(b)} \sum_{i=0}^{\infty}\sum_{j=0}^{\infty} \frac{(-1)^j \delta_i}{\Gamma(j+1)} \times \frac{\Gamma\left(\frac{1}{2}\left(2b+i+j+2L\min\left(m_1,m_2\right)\right)\right)}{\Gamma\left(i+2L\min\left(m_1,m_2\right)\right)\left(i+j+2L\min\left(m_1,m_2\right)\right)} \times \left(2\sqrt{\frac{\psi}{d\rho}}\right)^{2L\min(m_1,m_2)+i+j}. \quad (38)$$

[5]From here on, all changes in the order of integration are performed ensuring Fubini's conditions [75].

Finally, with the aid of [73, eq. (07.25.02.0001.01)] and after lengthy algebraic manipulations, an exact ABER expression is obtained as

$$P_{\mathrm{b}}^{\mathbb{R}^+\setminus\mathscr{A}} = \frac{\alpha^L 2^{-2L\min(m_1,m_2)-1}}{\Gamma(b)} \times \sum_{i=0}^{\infty} \frac{\delta_i \left(2\sqrt{\frac{\psi}{d\rho}}\right)^{2L\min(m_1,m_2)+i}}{\Gamma\left(i+2L\min\left(m_1,m_2\right)\right)} \left[\Theta_{1,i}\left(\rho\right) - \Theta_{2,i}\left(\rho\right)\right], \tag{39}$$

where

$$\Theta_{1,i}\left(\rho\right) = \frac{\Gamma\left(b+\frac{i}{2}+L\min\left(m_1,m_2\right)\right)}{\left(2L\min\left(m_1,m_2\right)+i\right)} \times {}_2F_2\Bigg(L\min\left(m_1,m_2\right)+\frac{i}{2}, L\min\left(m_1,m_2\right) + b+\frac{i}{2};\frac{1}{2}, L\min\left(m_1,m_2\right)+\frac{i}{2}+1;\frac{\psi}{d\rho}\Bigg) \tag{40}$$

$$\Theta_{2,i}\left(\rho\right) = \frac{2\sqrt{\frac{\psi}{d\rho}}\Gamma\left(b+\frac{i}{2}+L\min\left(m_1,m_2\right)+\frac{1}{2}\right)}{\left(2L\min\left(m_1,m_2\right)+i+1\right)} \times {}_2F_2\Bigg(L\min\left(m_1,m_2\right)+\frac{i}{2}+\frac{1}{2}, L\min\left(m_1,m_2\right) + b+\frac{i}{2}+\frac{1}{2};\frac{3}{2}, L\min\left(m_1,m_2\right)+\frac{i}{2}+\frac{3}{2};\frac{\psi}{d\rho}\Bigg). \tag{41}$$

On the other hand, the asymptotic ABER, can be readily obtained from (38) by taking the first (dominating) terms of both series, resulting in

$$P_{\mathrm{b}}^{\mathbb{R}^+\setminus\mathscr{A}} \simeq \left(\rho\,\mathcal{C}_b^*\right)^{-\mathcal{D}_b^*}, \tag{42}$$

where $\mathcal{D}_b^* = L\min\left(m_1,m_2\right)$ is the ABER diversity gain and

$$\mathcal{C}_b^* = \frac{d}{\psi}\left[\frac{\delta_0\alpha^L\Gamma\left(b+L\min\left(m_1,m_2\right)\right)}{2\Gamma(b)\Gamma\left(2L\min\left(m_1,m_2\right)+1\right)}\right]^{-\frac{1}{\mathcal{D}_b^*}} \tag{43}$$

the ABER coding gain.

2) Case II: A closed-form ABER expression can be obtaining by substituting (16) into (30), that is,

$$P_{\mathrm{b}}^{\mathscr{A}} = \frac{\beta^L}{2\Gamma(b)}\sum_{i=0}^{Lm^\dagger}\frac{\varphi_i}{\Gamma\left(i+2L\min\left(m_1,m_2\right)\right)}\mathcal{I}_i(\rho), \tag{44}$$

where $\mathcal{I}_i(\rho)$ is given by (37).

Thus, upon replacing (37) into (44), we have

$$P_{\mathrm{b}}^{\mathscr{A}} = \frac{\beta^L}{2\Gamma(b)}\sum_{i=0}^{Lm^\dagger}\sum_{j=0}^{\infty}\frac{(-1)^j\varphi_i\left(2\sqrt{\psi}\right)^{-2L\min(m_1,m_2)-i}}{\Gamma(j+1)\Gamma\left(i+2L\min\left(m_1,m_2\right)\right)} \times \frac{\Gamma\left(\frac{1}{2}\left(2b+i+j+2L\min\left(m_1,m_2\right)\right)\right)}{\left(i+j+2L\min\left(m_1,m_2\right)\right)} \times \left(2\sqrt{\frac{\psi}{d\rho}}\right)^{2L\min(m_1,m_2)+i+j}. \tag{45}$$

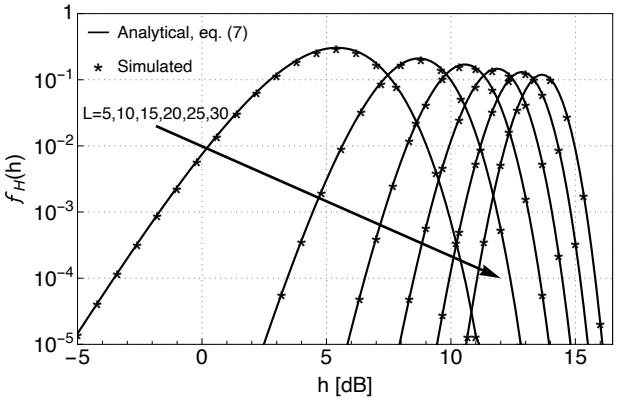

Fig. 2. PDF of H assuming $m_1 = 1.8$, $m_2 = 0.7$, $\Omega_1 = 1$, $\Omega_2 = 1$, and several values of L.

After several algebraic manipulations, an exact ABER expression can be finally obtained as

$$P_{\mathrm{b}}^{\mathscr{A}} = \frac{\beta^L}{2\Gamma(b)} \times \sum_{i=0}^{Lm^\dagger}\frac{\varphi_i\left(\sqrt{d\rho}\right)^{-2L\min(m_1,m_2)-i}}{\Gamma\left(i+2L\min\left(m_1,m_2\right)\right)}\left[\Theta_{1,i}\left(\rho\right)-\Theta_{2,i}\left(\rho\right)\right], \tag{46}$$

where $\Theta_{1,i}\left(\rho\right)$ and $\Theta_{2,i}\left(\rho\right)$ are given in (40) and (41), respectively.

An asymptotic closed-form ABER expressions can be promptly derived by using only the first (dominating) terms of the series in (45), yielding

$$P_{\mathrm{b}}^{\mathscr{A}} \simeq \left(\rho\,\mathcal{C}_b^\dagger\right)^{-\mathcal{D}_b^\dagger}, \tag{47}$$

where $\mathcal{D}_b^\dagger = L\min\left(m_1,m_2\right)$ is the ABER diversity gain and

$$\mathcal{C}_b^\dagger = d\left[\frac{\varphi_0\beta^L\Gamma\left(b+L\min\left(m_1,m_2\right)\right)}{2\Gamma(b)\Gamma\left(2L\min\left(m_1,m_2\right)+1\right)}\right]^{-\frac{1}{\mathcal{D}_b^\dagger}} \tag{48}$$

the ABER coding gain.

Notice that all diversity gains ($\mathcal{D}_{\text{out}}^*$, $\mathcal{D}_{\text{out}}^\dagger$, $\mathcal{D}_b^*$, and $\mathcal{D}_b^\dagger$) are equal to $L\min\left(m_1,m_2\right)$. Intuitively, this implies that the RIS-OPS enhances the system performance by choosing the most severe fading shape parameter between the two channels (S-RIS or RIS-D).

It is noteworthy to highlight that (22), (27), (39), and (46) are also original contributions of this work.

V. Numerical Results

Next, we corroborate the accuracy and efficiency of our analytical findings via Monte Carlo and numerical simulations.[6] The efficiency analysis is exclusively conducted for the PDF and CDF expressions outlined in Theorem 1 as they are not given in closed form.

[6]All simulations were conducted using MATHEMATICA software running on a standard laptop computer featuring a 12-core CPU comprising 6 performance cores and 6 efficiency cores, and unified memory of 18 GB.

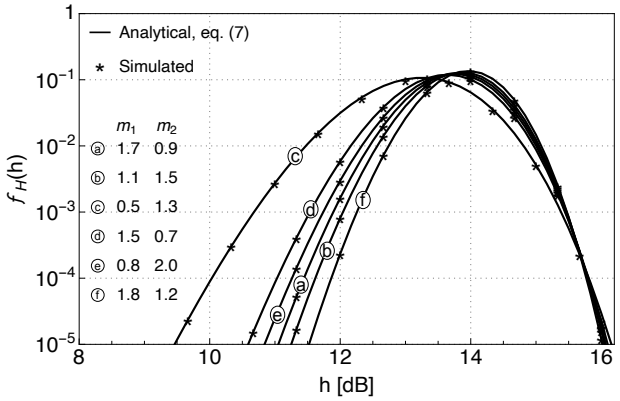

Fig. 3. PDF of H assuming $L = 30$, $\Omega_1 = 1$, $\Omega_2 = 1$, and several values of m_1 and m_2.

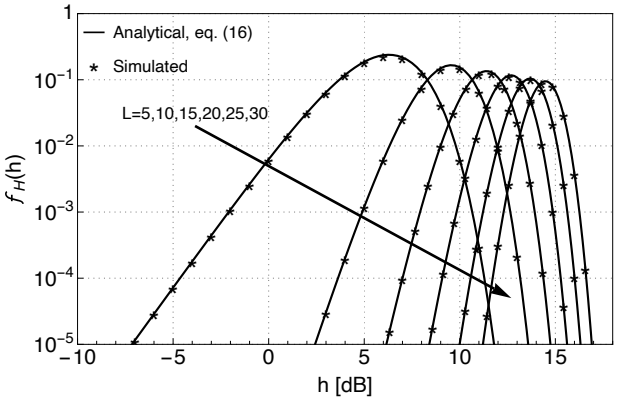

Fig. 4. PDF of H assuming $m_1 = 5$, $m_2 = 0.5$, $\Omega_1 = 1$, $\Omega_2 = 1$, and several values of L.

Figs. 2–5 illustrate the PDF of H computed through (7) and (16). In particular, Figs. 2 and 4 show the PDF of H for several values of L. Meanwhile Figs. 3 and 5 depict the PDF of H for different values of m_1 and m_2. The distribution parameters have been chosen to illustrate the wide range of shapes that the PDFs can exhibit. To plot Figs. 2 and 3, we utilized fewer than 200 terms in (7) and no more than 20 terms in (11). Notice the perfect agreement between the PDF curves and Monte Carlo simulations, thus corroborating our analytical findings.

Figs. 6 and 7 depict the exact and asymptotic OP expressions versus the average SNR per symbol for Case I and Case II, respectively, considering several values of L. Likewise, Figs. 8 and 9 show the exact and asymptotic ABER expressions versus the average SNR per symbol for Case I and Case II, respectively, considering different values of L. Observe in all the figures how the system performance improves as L increases, displaying lower OP and ABER values for a given average SNR per symbol. That is in agreement with our analytical findings since the OP and ABER diversity gains of both cases are proportional to L. Notice how our exact analytical curves perfectly coincide with the numerical simulations, offering robust validation for our results. Additionally, observe how our asymptotic formulations effectively describe the system behavior in the high SNR regime.

Figs. 10 and 11 respectively illustrate the elapsed times required by (7) and (8) to compute the PDF and the CDF of H versus the number of RIS elements L. Additionally, Figs. 10 and 11 consider the computation times required by the expressions outlined in [61] and [63]. As no PDF expressions were provided in [61] nor in [63], we calculate them using their corresponding CDFs. For the analysis, we consider an arbitrary single point $h = 10$, a target relative error of 10^{-10}, and four distinct parameter configurations. The integral expressions in [61] and [63] were evaluated using MATHEMATICA's numerical integration method "`GlobalAdaptive`"—which proved faster than the other available integration methods—with a

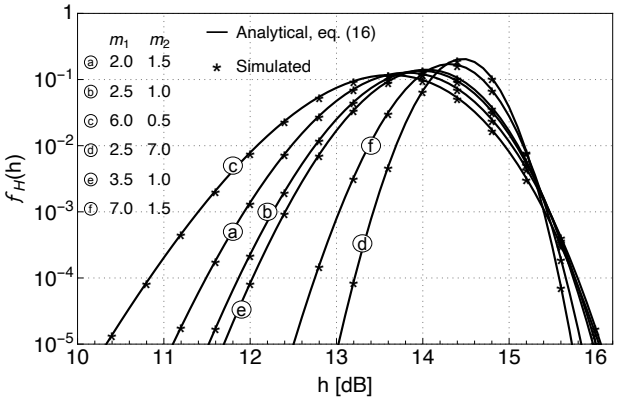

Fig. 5. PDF of H assuming $L = 30$, $\Omega_1 = 1$, $\Omega_2 = 1$, and several values of m_1 and m_2.

"`WorkingPrecision`" set to 100.[7] Notice in both figures that the elapsed times of the solutions in [63] significantly escalates with the increase in the number of RIS elements, evidencing computation times of above 10 seconds for $L = 3$, 100 seconds for $L = 6$, and surpassing 500 seconds for $L = 9$. The computation times of the solutions in [63] for $L \geq 12$ were not displayed because the numerical integration exhibited convergence instability issues or did not reach the target accuracy. Conversely, observe that the computation times of our solutions ((7) and (8)) as well as the ones given in [61] exhibit significant time reductions, showing elapsed times of less than 8 seconds for $3 \leq L \leq 30$. Also, notice that, although marginal, there is a gradual increase in computation time as L rises. Nonetheless, it can be easily infer that our expressions consistently offer the faster solution for any L.

Figs. 12 and 13 respectively show the relative errors of (7) and (8) versus their associated computation times. Figs. 12 and 13 also display the relative errors computed when using the solutions in [61]. Owing to instability concerns for $L > 10$ and the prolonged computation times involved ($\gg 10$ seconds), we refrain from conducting an accuracy analysis

[7]For low-dimensional integrals (our case), the accuracy goal is related to the "`WorkingPrecision`" parameter. In other words, the higher the "`WorkingPrecision`" parameter, the better the accuracy.

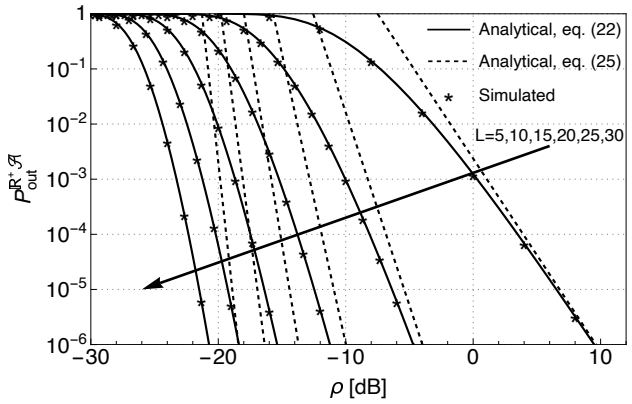

Fig. 6. OP (Case I) versus the average SNR per symbol, assuming $m_1 = 1.8$, $m_2 = 0.7$, $\Omega_1 = 1$, $\Omega_2 = 1$, $\gamma_{\text{th}} = 0$ [dB], and several values of L.

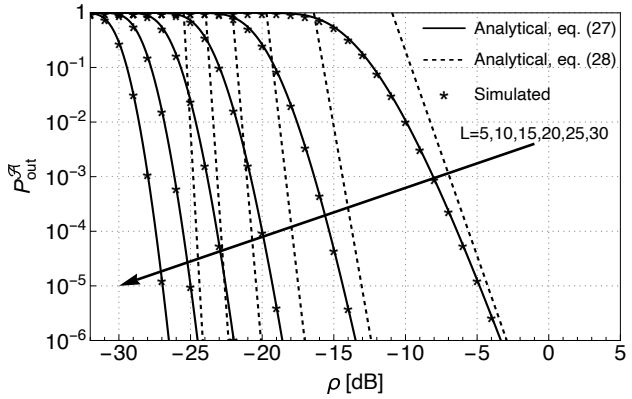

Fig. 7. OP (Case II) versus the average SNR per symbol, assuming $m_1 = 1.5$, $m_2 = 7$, $\Omega_1 = 1$, $\Omega_2 = 1$, $\gamma_{\text{th}} = 0$ [dB], and several values of L.

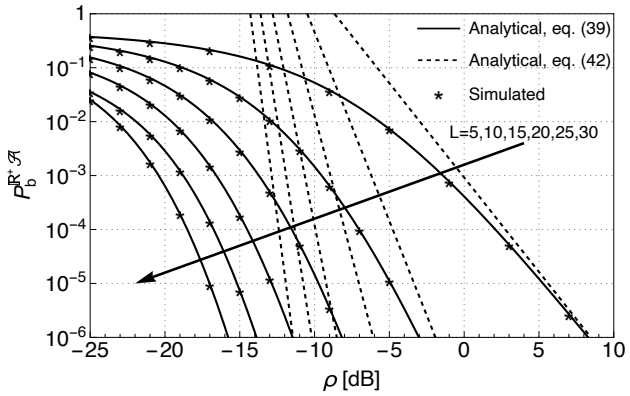

Fig. 8. ABER (Case I) versus the average SNR per symbol, assuming $m_1 = 4.7$, $m_2 = 1.1$, $\Omega_1 = 1$, $\Omega_2 = 1$, $b = 0.5$, $d = 1$, and several values of L.

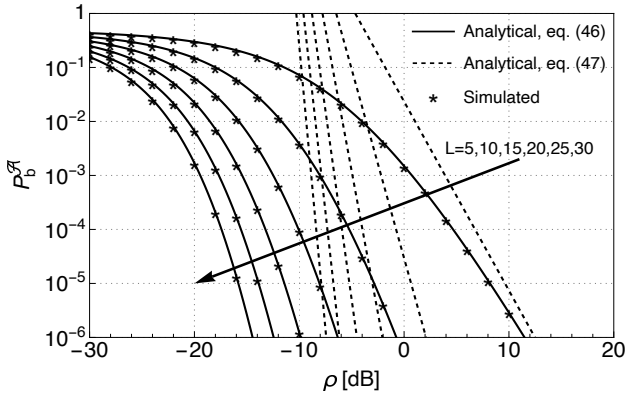

Fig. 9. ABER (Case II) versus the average SNR per symbol, assuming $m_1 = 3$, $m_2 = 2.5$, $\Omega_1 = 1$, $\Omega_2 = 1$, $b = 0.5$, $d = 1$, and several values of L.

for the formulations in [63]. In the figures, we consider an arbitrary single point $h = 10$, $m_1 = 3.2$, $m_2 = 1.7$, $\Omega_1 = 0.5$, $\Omega_2 = 1.5$, and different values of L. To calculate the relative errors in Figs. 12 and 13, we proceed as follows. When employing (7) and (8), we initially set the number of terms in (11) to 20, and subsequently start varying the number of terms in (7) and (8) from 20 to 350. Finally, for each iteration in the number of terms, we proceed to calculate the computation time and the corresponding relative error. On the other hand, when computing the expressions in [61], we vary the maximum total number of sample points used for the integration routine, "`MaxPoints`", from 10 up to 400.[8] Upon reaching the maximum number of evaluation points, the integration routine terminates. After the routine completion, we proceed to calculate the computation time and the associated relative error. Notice in both figures that the relative errors computed through [61] reach—due to machine precision—a lower limit independently of the computation time, where the solutions yield relative errors no less than 10^{-20}. In contrast, notice the fast convergence of (7) and (8) towards the ground truth, exhibiting a lower relative error for a given computation time. Furthermore, observe how the relative errors of (7) and (8) dramatically decrease as the computation time increases. For instance, for computation times between 2 and 4 seconds, (7) and (8) furnish outstanding relative errors, falling below 10^{-30}.

[8]The parameter "`MaxPoints`" sets the maximum number of evaluation points used in the numerical integration [73].

VI. Conclusions

This paper proposes new exact and tractable expressions for the channel statistics of a RIS-aided wireless communication system subject to Nakagami-m fading channels. The obtained PDF and CDF expressions represent the most efficient solutions reported in the technical literature to date. These expressions outperform the competing exact solutions in terms of accuracy, mathematical tractability, and computation time. We also carried out a performance assessment analysis, obtaining exact and asymptotic expressions for the OP and the ABER.

Appendix A
Proof of Theorem 1

To prove Theorem 1, we begin by employing the series representation of the modified Bessel function of the second

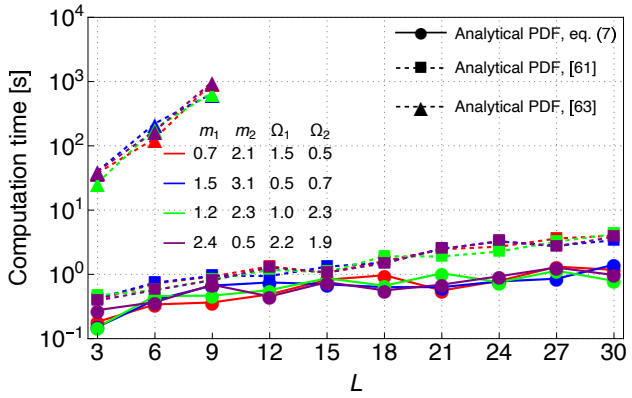

Fig. 10. Computation time of (7) versus the number of RIS elements L. The figure considers an arbitrary single point $h = 10$, a targeted relative error of less than 10^{-10}, and four distinct parameter configurations.

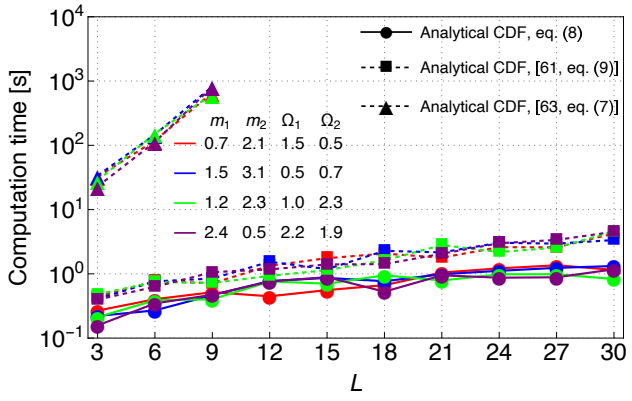

Fig. 11. Computation time of (8) versus the number of RIS elements L. The figure considers an arbitrary single point $h = 10$, a targeted relative error of less than 10^{-10}, and four distinct parameter configurations.

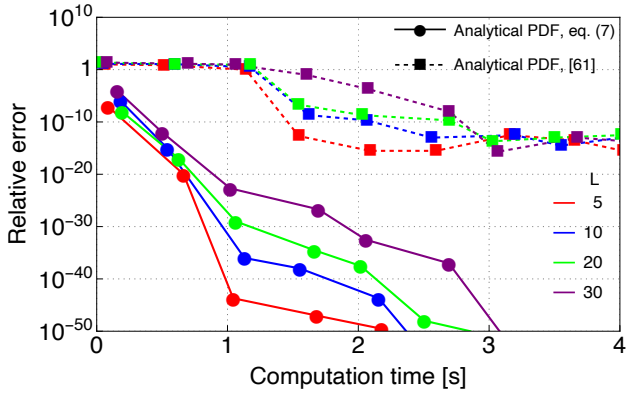

Fig. 12. Relative error versus the required computation time to calculate the PDF of H. The figure considers $|m_1 - m_2| \in \mathbb{R}^+ \setminus \mathscr{A}$, an arbitrary single point $h = 10$, $m_1 = 3.2$, $m_2 = 1.7$, $\Omega_1 = 0.5$, $\Omega_2 = 1.5$, and different values of L.

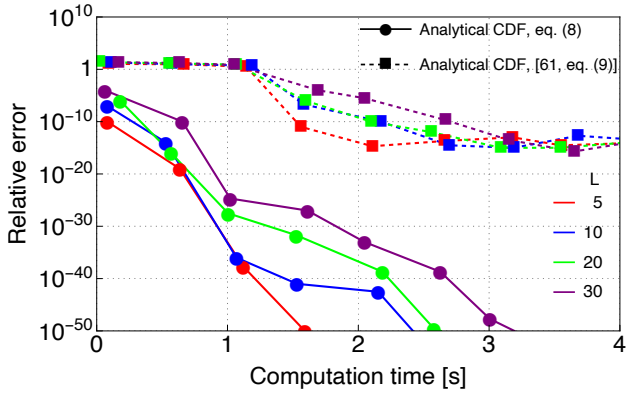

Fig. 13. Relative error versus the required computation time to calculate the CDF of H. The figure considers $|m_1 - m_2| \in \mathbb{R}^+ \setminus \mathscr{A}$, an arbitrary single point $h = 10$, $m_1 = 3.2$, $m_2 = 1.7$, $\Omega_1 = 0.5$, $\Omega_2 = 1.5$, and different values of L.

kind and νth order [77, eq. (6)]:

$$K_\nu(w) = \exp(-w)\frac{\sqrt{\pi}(2w)^{-\nu}\Gamma(2\nu)}{\Gamma\left(\frac{1}{2}-\nu\right)} \times \sum_{j=0}^{\infty}\sum_{i=0}^{j}\binom{j-1}{i-1}\frac{\Gamma\left(j-\nu+\frac{1}{2}\right)}{i!\Gamma\left(j+\nu+\frac{1}{2}\right)}(-2w)^i, \quad (49)$$

where $\nu \in \mathbb{R}^+ \setminus \mathscr{A}$.

Thereupon, from (49), we can rewrite (6) as

$$f_{H_\ell}(h_\ell) = \frac{\sqrt{\pi}4^{-m_1+m_2+1}\psi^{m_2}\Gamma\left(2\left(m_1-m_2\right)\right)h_\ell^{2m_2-1}}{\Gamma\left(m_1\right)\Gamma\left(m_2\right)\Gamma\left(-m_1+m_2+\frac{1}{2}\right)} \times \exp\left(-2\sqrt{\psi}h_\ell\right)\sum_{j=0}^{\infty}\sum_{i=0}^{j}\binom{i+j-1}{j-1} \times \frac{\Gamma\left(i+j-m_1+m_2+\frac{1}{2}\right)}{j!\Gamma\left(i+j+m_1-m_2+\frac{1}{2}\right)}\left(-4\sqrt{\psi}h_\ell\right)^j. \quad (50)$$

Noticing that we can equivalently define H_ℓ as the product of two Nakagami-m RVs with swapped PDF parameters (i.e., $H_\ell = h_{1,\ell}h_{2,\ell}$ with $h_{1,\ell} \sim \mathcal{NK}(m_2, \Omega_2)$ and $h_{2,\ell} \sim \mathcal{NK}(m_1, \Omega_1)$), and taking into account that the modified Bessel function of the second kind is an even function with respect to its parameter (i.e., $K_\nu(w) = K_{-\nu}(w)$), we can express (50) as

$$f_{H_\ell}(h_\ell) = \frac{\sqrt{\pi}4^{1-|m_1-m_2|}\Gamma\left(2\left|m_1-m_2\right|\right)\psi^{\min(m_1,m_2)}}{\Gamma\left(m_1\right)\Gamma\left(m_2\right)\Gamma\left(\frac{1}{2}-|m_1-m_2|\right)} \times h_\ell^{2\min(m_1,m_2)-1}\exp\left(-2\sqrt{\psi}h_\ell\right) \times \sum_{j=0}^{\infty}\sum_{i=0}^{j}\binom{i+j-1}{j-1}\frac{\Gamma\left(i+j-|m_1-m_2|+\frac{1}{2}\right)}{j!\Gamma\left(i+j+|m_1-m_2|+\frac{1}{2}\right)} \times \left(-4\sqrt{\psi}h_\ell\right)^j, \quad (51)$$

provided $|m_1 - m_2| \in \mathbb{R}^+ \setminus \mathscr{A}$.

Manipulating the summation indices in (51) along with some minor simplifications, we get

$$f_{H_\ell}(h_\ell) = \alpha\, h_\ell^{2\min(m_1,m_2)-1}\psi^{\min(m_1,m_2)}\exp\left(-2h_\ell\sqrt{\psi}\right) \times \sum_{i=0}^{\infty}\theta_i\left(-4\sqrt{\psi}h_\ell\right)^i, \quad (52)$$

where

$$\theta_i = \frac{1}{i!}\sum_{j=i}^{\infty}\binom{j-1}{i-1}\frac{\Gamma\left(j-|m_1-m_2|+\frac{1}{2}\right)}{\Gamma\left(j+|m_1-m_2|+\frac{1}{2}\right)}. \quad (53)$$

By the alternating series test [76] and since $f_{H_\ell}(h_\ell) < \infty$, we have $\lim_{i\to\infty}|\theta_i| = 0$.

Now, we proceed to take the Laplace transform of (52), i.e.,

$$\mathscr{L}\left\{f_{H_\ell}\right\}(s) = \int_0^{\infty}\exp\left(-sh_\ell\right) f_{H_\ell}(h_\ell)\,\mathrm{d}h_\ell, \quad (54)$$

in which $s \in \mathbb{C}$ and the integral converges provided $\mathbf{Re}\left[s\right] > 0$.

Plugging (52) into (54) and then solving the resulting integral, we obtain

$$\begin{aligned}\mathscr{L}\left\{f_{H_\ell}\right\}(s) =& \alpha\,\psi^{\min(m_1,m_2)} \\ &\times\sum_{i=0}^{\infty}\theta_i\left(s+2\sqrt{\psi}\right)^{-i-2\min(m_1,m_2)} \\ &\times\left(-4\sqrt{\psi}\right)^{i}\Gamma\left(i+2\min\left(m_1,m_2\right)\right). \quad (55)\end{aligned}$$

The proof of convergence of (55) is relegated to Appendix B.

As the sum in (4) is composed of i.i.d. double-Nakagami-m RVs,[9] then the Laplace transform of the PDF of H is given by

$$\mathscr{L}\left\{f_H\right\}(s) = \left[\mathscr{L}\left\{f_{H_\ell}\right\}(s)\right]^L. \quad (56)$$

Substituting (55) into (56), we get

$$\begin{aligned}\mathscr{L}\left\{f_H\right\}(s) =& \alpha^L\,\psi^{L\min(m_1,m_2)}\left(s+2\sqrt{\psi}\right)^{-2L\min(m_1,m_2)} \\ &\times\left[\sum_{i=0}^{\infty}\theta_i\left(\frac{s+2\sqrt{\psi}}{2\sqrt{\psi}}\right)^{-i}(-2)^i\,\Gamma\left(i+2\min\left(m_1,m_2\right)\right)\right]^L. \quad (57)\end{aligned}$$

Now, we aim at obtaining an equivalent single-series representation for (57). Thus, we employ a procedure akin to that outlined in [78]. In order to do so, we utilize the following differential equation:

$$\vartheta\left(\vartheta^L\right)' = L\vartheta^L\vartheta', \quad (58)$$

in which the prime symbol ($'$) signifies differentiation with respect to $\left(\left(s+2\sqrt{\psi}\right)/2\sqrt{\psi}\right)^{-1}$, and

$$\vartheta = \sum_{i=0}^{\infty}\theta_i\left(\frac{s+2\sqrt{\psi}}{2\sqrt{\psi}}\right)^{-i}(-2)^i\,\Gamma\left(i+2\min\left(m_1,m_2\right)\right) \quad (59)$$

$$\vartheta^L = \sum_{i=0}^{\infty}\delta_i\left(\frac{s+2\sqrt{\psi}}{2\sqrt{\psi}}\right)^{-i}. \quad (60)$$

Notice that (59) is the series inside the square brackets in (57).

After solving (58) through recursive steps and subsequently performing certain algebraic simplifications, it can be deduced that the coefficients δ_i required in (60) can ultimately be written as in (10).

[9]A double-Nakagami-m distribution is formed by the product of two independent and not identically distributed Nakagami-m RVs [49].

Utilizing (60) in (57), we obtain

$$\begin{aligned}\mathscr{L}\left\{f_H\right\}(s) =& \alpha^L\,\psi^{L\min(m_1,m_2)}\left(s+2\sqrt{\psi}\right)^{-2L\min(m_1,m_2)} \\ &\times\sum_{i=0}^{\infty}\delta_i\left(\frac{s+2\sqrt{\psi}}{2\sqrt{\psi}}\right)^{-i}. \quad (61)\end{aligned}$$

Notice in (56) and (57) that in order to compute $\mathscr{L}\left\{f_H\right\}(s)$, we raised a convergent series to the power of L. Therefore, the resulting series in (61) is also convergent, implying that

$$\lim_{i\to\infty}|\delta_i| = 0. \quad (62)$$

Now, we employ the Fourier-Mellin integral to perform the Laplace inversion [79]:

$$f_H(h) = \frac{1}{2\pi\,\mathrm{i}}\oint_{\mathcal{L}_\mathrm{B}}\exp(sh)\mathscr{L}\left\{f_H\right\}(s)\mathrm{d}s, \quad (63)$$

where $\mathcal{L}_\mathrm{B}$ denotes the Bromwich contour.

Replacing (61) into (63), we obtain

$$\begin{aligned}f_H(h) =& \frac{\alpha^L\,\psi^{L\min(m_1,m_2)}}{2\pi\,\mathrm{i}}\oint_{\mathcal{L}_\mathrm{B}}\exp(sh) \\ &\times\sum_{i=0}^{\infty}\delta_i\left(2\sqrt{\psi}\right)^{i}\left(s+2\sqrt{\psi}\right)^{-i-2L\min(m_1,m_2)}\mathrm{d}s. \quad (64)\end{aligned}$$

Finally, after performing a term-by-term inversion with the assistance of [70, eq. (29.3.10)], the PDF of H can be derived as in (7).

The CDF of H can be promptly obtained after integrating (7) from zero to h, i.e., $F_H(h) = \int_0^h f_H(u)\mathrm{d}u$, yielding (8). This completes the proof.

Appendix B
Convergence of (55)

In the pursuit of establishing the convergence of (55), our initial step involves deriving the raw moments of H_ℓ, defined as

$$\mathcal{M}_n \triangleq \mathbb{E}\left[H_\ell^n\right] = \int_0^{\infty}h_\ell^n f_{H_\ell}(h_\ell)\mathrm{d}h_\ell, \quad (65)$$

where $n \in \mathbb{N}$. As the raw moments of $h_{1,\ell}$ and $h_{2,\ell}$ exist, it implies that the raw moments of H_ℓ also exist (i.e., $\mathcal{M}_n < \infty$).

Replacing (52) into (65) and then evaluating the resulting integral with the assistance of [73, eq. (06.05.02.0001.01)], we obtain

$$\begin{aligned}\mathcal{M}_n =& \alpha\,\psi^{\min(m_1,m_2)}\left(2\sqrt{\psi}\right)^{-2\min(m_1,m_2)-n} \\ &\times\sum_{i=0}^{\infty}\theta_i(-2)^i\Gamma\left(i+n+2\min\left(m_1,m_2\right)\right). \quad (66)\end{aligned}$$

Applying alternating series test [76] in (66), it follows that

$$\lim_{i\to\infty}|\theta_i| = 0. \quad (67)$$

Furthermore, it implies that $|\theta_i|$ must eventually decay faster than $\left[2^i\Gamma\left(i+n+2\min\left(m_1,m_2\right)\right)\right]^{-1}$, namely, there exists an $r_\theta \in \mathbb{N}$ such that

$$\sup_i \left\{|\theta_i|\, 2^i\Gamma\left(i+n+2\min\left(m_1,m_2\right)\right)\right\} = 1, \quad i > r_\theta. \tag{68}$$

In order for the Laplace transform of $f_{H_\ell}(h_\ell)$ to converge, it is necessary that [79]:

$$\left|\mathscr{L}\left\{f_{H_\ell}\right\}(s)\right| < \infty. \tag{69}$$

Using (55) as well as the triangle inequality, $\left|\mathscr{L}\left\{f_{H_\ell}\right\}(s)\right|$ can be bounded as

$$\begin{aligned}\left|\mathscr{L}\left\{f_{H_\ell}\right\}(s)\right| < \alpha\, \psi^{\min(m_1,m_2)} \left(s+2\sqrt{\psi}\right)^{-2\min(m_1,m_2)} \\ \times \sum_{i=0}^{\infty} |\theta_i| \left(\frac{s+2\sqrt{\psi}}{2\sqrt{\psi}}\right)^{-i} 2^i\Gamma\left(i+2\min\left(m_1,m_2\right)\right).\end{aligned} \tag{70}$$

Applying (68) in (70), we have

$$\begin{aligned}\left|\mathscr{L}\left\{f_{H_\ell}\right\}(s)\right| <& \alpha\, \psi^{\min(m_1,m_2)} \left(s+2\sqrt{\psi}\right)^{-2\min(m_1,m_2)} \\ & \times \sum_{i=0}^{\infty} \left(\frac{s}{2\sqrt{\psi}}+1\right)^{-i}.\end{aligned} \tag{71}$$

Taking into account that $(s/2\sqrt{\psi})+1 > 1$ for $\mathbf{Re}\left[s\right] > 0$, the series in (71) can be evaluated in closed form, yielding

$$\begin{aligned}&\left|\mathscr{L}\left\{f_{H_\ell}\right\}(s)\right| \\ &\quad < \alpha\, \psi^{\min(m_1,m_2)} s^{-1} \left(s+2\sqrt{\psi}\right)^{1-2\min(m_1,m_2)}.\end{aligned} \tag{72}$$

Thus, as the upper bound in (72) exists, the convergence of (55) is ensured. This completes the proof.

Appendix C
Absolute and Uniform Convergence of (7)

Define $\mathcal{H}(h)$ as a function with a similar analytical structure to (7), but it takes the absolute value of the summands, namely

$$\begin{aligned}\mathcal{H}(h) \triangleq& \alpha^L h^{-1} \exp\left(-2h\sqrt{\psi}\right) \\ & \times \sum_{i=0}^{\infty} \left|\frac{2^i\delta_i \left(h\sqrt{\psi}\right)^{2L\min(m_1,m_2)+i}}{\Gamma\left(i+2L\min\left(m_1,m_2\right)\right)}\right|.\end{aligned} \tag{73}$$

Thus, if (73) converges, then (7) converges absolutely [76].

Applying the absolute value operator in (73), we have

$$\begin{aligned}\mathcal{H}(h) =& \alpha^L h^{-1} \exp\left(-2h\sqrt{\psi}\right) \\ & \times \sum_{i=0}^{\infty} \frac{2^i\left|\delta_i\right| \left(h\sqrt{\psi}\right)^{2L\min(m_1,m_2)+i}}{\Gamma\left(i+2L\min\left(m_1,m_2\right)\right)}.\end{aligned} \tag{74}$$

Using (62), we can define $\delta^* \triangleq \max_i\left\{|\delta_i|\right\}$. Accordingly, we are now able to establish an upper bound for $\mathcal{H}(h)$ as

$$\begin{aligned}\mathcal{H}(h) <& \alpha^L h^{-1}\delta^* \exp\left(-2h\sqrt{\psi}\right) \\ & \times \sum_{i=0}^{\infty} \frac{2^i \left(h\sqrt{\psi}\right)^{2L\min(m_1,m_2)+i}}{\Gamma\left(i+2L\min\left(m_1,m_2\right)\right)}.\end{aligned} \tag{75}$$

By applying [70, eq. (6.5.12)], we can obtain a closed-form expression for the bound in (75), given by

$$\begin{aligned}\mathcal{H}(h) <& \sqrt{\psi}\, \alpha^L\, \delta^* 2^{1-2L\min(m_1,m_2)} \\ & \times \frac{\Upsilon\left(2L\min\left(m_1,m_2\right)-1, 2h\sqrt{\psi}\right)}{\Gamma\left(2L\min\left(m_1,m_2\right)-1\right)}.\end{aligned} \tag{76}$$

Therefore, given the existence of an upper bound for $\mathcal{H}(h)$, it follows that (73) converges and (7) converges absolutely.

After employing $0 \le \frac{\Upsilon(a,h)}{\Gamma(h)} < 1$ for $h \ge 0$ in (76), we can still establish an upper bound for $\mathcal{H}(h)$ as

$$\mathcal{H}(h) < \delta^* \sqrt{\psi} \alpha^L 2^{1-2L\min(m_1,m_2)}, \tag{77}$$

Notice in (77) that it exits an upper bound for $\mathcal{H}(h)$ is independent of h. Therefore, by the Weierstrass M-test [80], we conclude that (7) converges uniformly and absolutely on h. This completes the proof.

Appendix D
Truncation Error Bound for (12)

Similar to Appendix D, we leverage the existence of $r_\delta \in \mathbb{N}$ such that $\sup_i |\delta_i| = 1$ holds for every i greater than r_δ. Hence, the truncation error in (13) can be bounded as

$$\begin{aligned}\epsilon_{f_H}(h) <& \frac{\alpha^L \exp\left(-2h\sqrt{\psi}\right)}{h} \\ & \times \sum_{i=t}^{\infty} \frac{2^i \left(h\sqrt{\psi}\right)^{2L\min(m_1,m_2)+i}}{\Gamma\left(i+2L\min\left(m_1,m_2\right)\right)}.\end{aligned} \tag{78}$$

By direct application of [70, eq. (6.5.12)], an upper bound for $\epsilon_{f_H}(h)$ can be obtained in closed form as in (14), thereby finalizing the proof.

Appendix E
Truncation Error Bound for (13)

Similar to Appendix D, we leverage the existence of $r_\delta \in \mathbb{N}$ such that $\sup_i |\delta_i| = 1$ holds for every i greater than r_δ. Hence, the truncation error in (13) can be bounded as

$$\begin{aligned}\epsilon_{F_H}(h) <& \alpha^L 4^{-L\min(m_1,m_2)} \\ & \times \sum_{i=t}^{\infty} \frac{\Upsilon\left(2L\min\left(m_1,m_2\right)+i, 2h\sqrt{\psi}\right)}{\Gamma\left(2L\min\left(m_1,m_2\right)+i\right)}.\end{aligned} \tag{79}$$

Applying the upper bound for the lower incomplete gamma given in [81, Theorem 4.1], we have

$$\begin{aligned}\epsilon_{F_H}(h) <& \alpha^L 4^{-L\min(m_1,m_2)} \left(2h\sqrt{\psi}\right)^{2L\min(m_1,m_2)} \\ & \times \sum_{i=t}^{\infty} \frac{\left(\left(2L\min\left(m_1,m_2\right)+i\right)\exp\left(-2h\sqrt{\psi}\right)+1\right)}{\Gamma\left(i+2L\min\left(m_1,m_2\right)+2\right)} \\ & \times \left(2h\sqrt{\psi}\right)^{i} \\ <& \alpha^L 4^{-L\min(m_1,m_2)} \left(2h\sqrt{\psi}\right)^{2L\min(m_1,m_2)} \\ & \times \sum_{i=t}^{\infty} \frac{\left(\left(2L\min\left(m_1,m_2\right)+i\right)+1\right)}{\Gamma\left(i+2L\min\left(m_1,m_2\right)+2\right)} \left(2h\sqrt{\psi}\right)^{i}.\end{aligned} \tag{80}$$

Ultimately, the infinite summation in (80) can be evaluated in close form with the aid of [70, eq. (6.5.12)], yielding (15), thus completing the proof.

APPENDIX F
PROOF OF THEOREM 2

We commence by utilizing the finite sum representation of the modified Bessel function of the second kind and νth order [73, eq. (03.04.03.0004.01)]:

$$K_{\nu}(w)=\sqrt{\frac{\pi}{2w}}\exp(-w)\sum_{i=0}^{\lfloor |\nu|-\frac{1}{2}\rfloor}\frac{\left(i+|\nu|-\frac{1}{2}\right)!}{i!\left(-i+|\nu|-\frac{1}{2}\right)!}(2w)^{-i}, \tag{81}$$

which is valid for $\nu\in\mathbb{Z}+\frac{1}{2}$.

By employing (81) and the relationship $K_{\nu}(w)=K_{-\nu}(w)$, we can express (6) as

$$f_{H_{\ell}}\left(h_{\ell}\right)=\frac{2\sqrt{\pi}\sqrt{\psi}^{m_1+m_2-\frac{1}{2}}h_{\ell}^{m_1+m_2-\frac{3}{2}}}{\Gamma\left(m_1\right)\Gamma\left(m_2\right)}\exp\left(-2\sqrt{\psi}h_{\ell}\right)\times\sum_{j=0}^{m^{\dagger}}\frac{\left(4\sqrt{\psi}h_{\ell}\right)^{-j}\left(|m_1-m_2|+j-\frac{1}{2}\right)!}{j!\left(|m_1-m_2|-j-\frac{1}{2}\right)!}, \tag{82}$$

provided $|m_1-m_2|\in\mathbb{N}-\frac{1}{2}$.

Changing the index of summation $i\rightarrow(m^{\dagger}-j)$ and using the fact that $\left(-\left\lfloor a-\frac{1}{2}\right\rfloor-\frac{1}{2}\right)!=\Gamma\left(\left\lceil\frac{1}{2}-a\right\rceil+\frac{1}{2}\right)$, we can rewrite (82) as

$$f_{H_{\ell}}\left(h_{\ell}\right)=\frac{2\sqrt{\pi}\sqrt{\psi}^{m_1+m_2-\frac{1}{2}}h_{\ell}^{m_1+m_2-\frac{3}{2}}}{\Gamma\left(m_1\right)\Gamma\left(m_2\right)}\exp\left(-2\sqrt{\psi}h_{\ell}\right)\times\sum_{i=0}^{m^{\dagger}}\frac{\left(4\sqrt{\psi}h_{\ell}\right)^{i-m^{\dagger}}\Gamma\left(-i+|m_1-m_2|+m^{\dagger}+\frac{1}{2}\right)}{\Gamma\left(-i+m^{\dagger}+1\right)\Gamma\left(m^{\ddagger}+i+|m_1-m_2|+\frac{1}{2}\right)}. \tag{83}$$

Applying the Laplace transform to (83), we get

$$\mathscr{L}\left\{f_{H_{\ell}}\right\}(s)=\frac{2\sqrt{\pi}\sqrt{\psi}^{m_1+m_2-\frac{1}{2}}}{\Gamma\left(m_1\right)\Gamma\left(m_2\right)}\times\sum_{i=0}^{m^{\dagger}}\phi_i\left(s+2\sqrt{\psi}\right)^{-i-m^{\ddagger}-m_1-m_2+\frac{1}{2}}\times\left(4\sqrt{\psi}\right)^{i-m^{\dagger}}\Gamma\left(m^{\ddagger}+i+m_1+m_2-\frac{1}{2}\right), \tag{84}$$

where

$$\phi_i=\frac{\Gamma\left(-i+|m_1-m_2|+m^{\dagger}+\frac{1}{2}\right)}{\Gamma\left(-i+m^{\dagger}+1\right)\Gamma\left(m^{\ddagger}+i+|m_1-m_2|+\frac{1}{2}\right)}. \tag{85}$$

The Laplace transform of the PDF of X is obtaining by substituting (84) into (56), yielding

$$\mathscr{L}\left\{f_H\right\}(s)=\beta^L\,\phi_i\left(s+2\sqrt{\psi}\right)^{L\left(-m^{\ddagger}-m_1-m_2+\frac{1}{2}\right)}\times\left[\sum_{i=0}^{m^{\dagger}}\phi_i\left(s+2\sqrt{\psi}\right)^{-i}\left(4\sqrt{\psi}\right)^{i}\times\Gamma\left(m^{\ddagger}+i+m_1+m_2-\frac{1}{2}\right)\right]^{L}. \tag{86}$$

Exploiting the fact that $m^{\ddagger}+m_1+m_2-\frac{1}{2}=2\min\left(m_1,m_2\right)$ holds when $|m_1-m_2|\in\mathbb{N}-\frac{1}{2}$, we can rewrite (86) as

$$\mathscr{L}\left\{f_H\right\}(s)=\beta^L\,\phi_i\left(s+2\sqrt{\psi}\right)^{-2L\min(m_1,m_2)}\times\left[\sum_{i=0}^{m^{\dagger}}\phi_i\left(s+2\sqrt{\psi}\right)^{-i}\left(4\sqrt{\psi}\right)^{i}\times\Gamma\left(2\min\left(m_1,m_2\right)+i\right)\right]^{L}. \tag{87}$$

Notice that (57) and (87) have a similar analytical structure. Hence, we can apply the same rationale to obtain an equivalent sum representation for (86). Thus, we consider the following differential equation:

$$\varsigma\left(\varsigma^{L}\right)'=L\varsigma^{L}\varsigma', \tag{88}$$

where, as in (58), the prime symbol ($'$) signifies differentiation with respect to $\left(s+2\sqrt{\psi}\right)^{-1}$. Moreover,

$$\varsigma=\sum_{i=0}^{m^{\dagger}}\phi_i\left(s+2\sqrt{\psi}\right)^{-i}\left(4\sqrt{\psi}\right)^{i}\Gamma\left(2\min\left(m_1,m_2\right)+i\right) \tag{89}$$

$$\varsigma^{L}=\sum_{i=0}^{Lm^{\dagger}}\varphi_i\left(s+2\sqrt{\psi}\right)^{-i}. \tag{90}$$

Notice that (89) is the finite sum inside the square brackets in (86). Furthermore, notice that unlike (60), we choose (90) to be a finite sum with limit of summation equal to $Lm^{\dagger}$. That is because when we raise a polynomial of degree $m^{\dagger}$ to the Lth power [refer to (86)], the maximum exponent of the resulting polynomial is $Lm^{\dagger}$.

By solving the differential equation (88) through recursive steps and followed by some algebraic manipulations, it follows that the coefficients φ_i needed in (90) can be computed as in (19).

Employing (90) in (86), we obtain

$$\mathscr{L}\left\{f_H\right\}(s)=\beta^L\left(s+2\sqrt{\psi}\right)^{-2L\min(m_1,m_2)}\times\sum_{i=0}^{Lm^{\dagger}}\varphi_i\left(s+2\sqrt{\psi}\right)^{-i}. \tag{91}$$

The PDF of H can be obtained replacing (91) into (63), namely,

$$f_H(h)=\frac{\beta^L}{2\pi\,\mathrm{i}}\oint_{\mathcal{L}_{\mathrm{B}}}\exp(sh)\times\sum_{i=0}^{Lm^{\dagger}}\varphi_i\left(s+2\sqrt{\psi}\right)^{-i-2L\min(m_1,m_2)}\mathrm{d}s. \tag{92}$$

After a term-by-term inversion with the aid of [70, eq. (29.3.10)], the PDF of H can be derived as in (16), whereas the CDF of H can be obtained after integrating (16) from zero to h, yielding (17). This completes the proof.

REFERENCES

[1] Q. Wu and R. Zhang, "Towards smart and reconfigurable environment: Intelligent reflecting surface aided wireless network," *IEEE Commun. Mag.*, vol. 58, no. 1, pp. 106–112, Nov. 2020.

[2] S. Noh, J. Lee, G. Lee, K. Seo, Y. Sung, and H. Yu, "Channel estimation techniques for RIS-assisted communication: Millimeter-wave and sub-THz systems," *IEEE Veh. Technol. Mag.*, vol. 17, no. 2, pp. 64–73, Jun. 2022.

[3] C. Huang, A. Zappone, G. C. Alexandropoulos, M. Debbah, and C. Yuen, "Reconfigurable intelligent surfaces for energy efficiency in wireless communication," *IEEE Trans. Wireless Commun.*, vol. 18, no. 8, pp. 4157–4170, Aug. 2019.

[4] E. Basar, M. Di Renzo, J. De Rosny, M. Debbah, M. S. Alouini, and R. Zhang, "Wireless communications through reconfigurable intelligent surfaces," *IEEE Access*, vol. 7, pp. 116 753–116 773, Aug. 2019.

[5] X. Qian, M. Di Renzo, J. Liu, A. Kammoun, and M.-S. Alouini, "Beamforming through reconfigurable intelligent surfaces in single-user MIMO systems: SNR distribution and scaling laws in the presence of channel fading and phase noise," *IEEE Wireless Commun. Lett.*, vol. 10, no. 1, pp. 77–81, Jan. 2021.

[6] T. Hou, Y. Liu, Z. Song, X. Sun, Y. Chen, and L. Hanzo, "MIMO assisted networks relying on intelligent reflective surfaces: A stochastic geometry based analysis," *IEEE Trans. Veh. Technol.*, vol. 71, no. 1, pp. 571–582, Jan. 2022.

[7] Z. Ding, R. Schober, and H. V. Poor, "On the impact of phase shifting designs on IRS-NOMA," *IEEE Wireless Commun. Lett.*, vol. 9, no. 10, pp. 1596–1600, Oct. 2020.

[8] L. Yang, F. Meng, J. Zhang, M. O. Hasna, and M. D. Renzo, "On the performance of RIS-assisted dual-hop UAV communication systems," *IEEE Trans. Veh. Technol.*, vol. 69, no. 9, pp. 10 385–10 390, Sep. 2020.

[9] E. K. Agbogla, I. Trigui, K. Humadi, W. Ajib, and W.-P. Zhu, "Adaptive coordinated direct and multi-RIS transmissions for ultrareliable terahertz systems," *IEEE Trans. Veh. Technol.*, vol. 72, no. 8, pp. 10 988–10 993, Aug. 2023.

[10] L. Yuan, Q. Du, N. Yang, F. Fang, and N. Yang, "Performance analysis of IRS-aided short-packet NOMA systems over Nakagami-m fading channels," *IEEE Trans. Veh. Technol.*, vol. 72, no. 6, pp. 8228–8233, Jun. 2023.

[11] M. Hamza Naim Shaikh, V. Ashok Bohara, A. Srivastava, and G. Ghatak, "On the performance of RIS-aided NOMA system with non-ideal transceiver over Nakagami-m fading," in *Proc. IEEE Wireless Commun. Netw. Conf. (WCNC)*, Austin, TX, USA, Apr. 2022, pp. 1737–1742.

[12] B. Tahir, S. Schwarz, and M. Rupp, "Analysis of uplink IRS-assisted NOMA under Nakagami-m fading via moments matching," *IEEE Wireless Commun. Lett.*, vol. 10, no. 3, pp. 624–628, Mar. 2021.

[13] B. C. Nguyen, L. T. Dung, T. M. Hoang, N. V. Vinh, and G. T. Luu, "On performance of multi-RIS assisted multi-user nonorthogonal multiple access system over Nakagami-m fading channels," *Comput. Commun.*, vol. 197, pp. 294–305, Jan. 2023.

[14] M. H. N. Shaikh, S. Arzykulov, A. Celik, A. M. Eltawil, and G. Nauryzbayev, "Performance of RIS-empowered NOMA-based D2D communication under Nakagami-m fading," in *Proc. IEEE 96th Veh. Technol. Conf. (VTC)*, London, United Kingdom, Sep. 2022, pp. 1–5.

[15] C. Zhang, W. Yi, Y. Liu, K. Yang, and Z. Ding, "Reconfigurable intelligent surfaces aided multi-cell NOMA networks: A stochastic geometry model," *IEEE Trans. Commun.*, vol. 70, no. 2, pp. 951–966, Feb. 2022.

[16] Z. Tang, T. Hou, Y. Liu, J. Zhang, and L. Hanzo, "Physical layer security of intelligent reflective surface aided NOMA networks," *IEEE Trans. Veh. Technol.*, vol. 71, no. 7, pp. 7821–7834, Jul. 2022.

[17] Y. Cheng, K. H. Li, Y. Liu, K. C. Teh, and H. Vincent Poor, "Downlink and uplink intelligent reflecting surface aided networks: NOMA and OMA," *IEEE Trans. Wireless Commun.*, vol. 20, no. 6, pp. 3988–4000, Jun. 2021.

[18] H. Du, J. Zhang, K. Guan, D. Niyato, H. Jiao, Z. Wang, and T. Kürner, "Performance and optimization of reconfigurable intelligent surface aided THz communications," *IEEE Trans. Commun.*, vol. 70, no. 5, pp. 3575–3593, May 2022.

[19] N. P. Le and M.-S. Alouini, "Performance analysis of RIS-aided THz wireless systems over α-μ fading: An approximate closed-form approach," *IEEE Internet Things J.*, early access, Jun. 22, 2023, doi: 10.1109/JIOT.2023.3288588.

[20] A.-A. A. Boulogeorgos, A. Alexiou, and M. D. Renzo, "Outage performance analysis of RIS-assisted UAV wireless systems under disorientation and misalignment," *IEEE Trans. Veh. Technol.*, vol. 71, no. 10, pp. 10 712–10 728, Oct. 2022.

[21] W. Shi, J. Xu, W. Xu, M. D. Renzo, and C. Zhao, "Secure outage analysis of RIS-assisted communications with discrete phase control," *IEEE Trans. Veh. Technol.*, vol. 72, no. 4, pp. 5435–5440, Apr. 2023.

[22] D. Kudathanthirige, D. Gunasinghe, and G. Amarasuriya, "Performance analysis of intelligent reflective surfaces for wireless communication," in *Proc. IEEE Int. Conf. Commun. (ICC)*, Dublin, Ireland, Jun. 2020, pp. 1–6.

[23] L. Yang, Y. Yang, M. O. Hasna, and M.-S. Alouini, "Coverage, probability of SNR gain, and DOR analysis of RIS-aided communication systems," *IEEE Wireless Commun. Lett.*, vol. 9, no. 8, pp. 1268–1272, Aug. 2020.

[24] Y. Ai, F. A. P. deFigueiredo, L. Kong, M. Cheffena, S. Chatzinotas, and B. Ottersten, "Secure vehicular communications through reconfigurable intelligent surfaces," *IEEE Trans. Veh. Technol.*, vol. 70, no. 7, pp. 7272–7276, Jul. 2021.

[25] Y. Zhang, J. Zhang, M. D. Renzo, H. Xiao, and B. Ai, "Performance analysis of RIS-aided systems with practical phase shift and amplitude response," *IEEE Trans. Veh. Technol.*, vol. 70, no. 5, pp. 4501–4511, May 2021.

[26] L. Kong, S. Kisseleff, S. Chatzinotas, B. Ottersten, and M. Erol-Kantarci, "Effective rate of RIS-aided networks with location and phase estimation uncertainty," in *Proc. IEEE Wireless Commun. Netw. Conf. (WCNC)*, Austin, TX, USA, Apr. 2022, pp. 2071–2075.

[27] Y. Bian, D. Dong, J. Jiang, and K. Song, "Performance analysis of reconfigurable intelligent surface-assisted wireless communication systems under co-channel interference," *IEEE Open J. Commun. Soc.*, vol. 4, pp. 596–605, Feb. 2023.

[28] Z. Cui, K. Guan, J. Zhang, and Z. Zhong, "SNR coverage probability analysis of RIS-aided communication systems," *IEEE Trans. Veh. Technol.*, vol. 70, no. 4, pp. 3914–3919, Apr. 2021.

[29] S. Dhok and P. K. Sharma, "Infinite and finite block-length FD transmissions with spatially-correlated RIS channels," *IEEE Trans. Wireless Commun.*, vol. 22, no. 2, pp. 1060–1071, Feb. 2023.

[30] S. Atapattu, R. Fan, P. Dharmawansa, G. Wang, J. Evans, and T. A. Tsiftsis, "Reconfigurable intelligent surface assisted two–way communications: Performance analysis and optimization," *IEEE Trans. Commun.*, vol. 68, no. 10, pp. 6552–6567, Oct. 2020.

[31] A.-A. A. Boulogeorgos and A. Alexiou, "Performance analysis of reconfigurable intelligent surface-assisted wireless systems and comparison with relaying," *IEEE Access*, vol. 8, pp. 94 463–94 483, May 2020.

[32] L. Yang, Y. Yang, D. B. d. Costa, and I. Trigui, "Outage probability and capacity scaling law of multiple RIS-aided networks," *IEEE Wireless Commun. Lett.*, vol. 10, no. 2, pp. 256–260, Feb. 2021.

[33] P. Xu, G. Chen, Z. Yang, and M. D. Renzo, "Reconfigurable intelligent surfaces-assisted communications with discrete phase shifts: How many quantization levels are required to achieve full diversity?" *IEEE Wireless Commun. Lett.*, vol. 10, no. 2, pp. 358–362, Feb. 2021.

[34] J. Lyu and R. Zhang, "Spatial throughput characterization for intelligent reflecting surface aided multiuser system," *IEEE Wireless Commun. Lett.*, vol. 9, no. 6, pp. 834–838, Jun. 2020.

[35] E. Björnson and L. Sanguinetti, "Rayleigh fading modeling and channel hardening for reconfigurable intelligent surfaces," *IEEE Wireless Commun. Lett.*, vol. 10, no. 4, pp. 830–834, Apr. 2021.

[36] T. Wang, G. Chen, J. P. Coon, and M.-A. Badiu, "Chernoff bound and saddlepoint approximation for outage probability in IRS-assisted wireless systems," in *Proc. IEEE Globecom Workshops (GC Wkshps)*, Madrid, Spain, Dec. 2021, pp. 1–5.

[37] T. Van Chien, A. K. Papazafeiropoulos, L. T. Tu, R. Chopra, S. Chatzinotas, and B. Ottersten, "Outage probability analysis of IRS-assisted systems under spatially correlated channels," *IEEE Wireless Commun. Lett.*, vol. 10, no. 8, pp. 1815–1819, Aug. 2021.

[38] T. Wang, G. Chen, J. P. Coon, and M.-A. Badiu, "Study of intelligent reflective surface assisted communications with one-bit phase adjustments," in *Proc. IEEE Global Commun. Conf. (Globecom)*, Taipei, Taiwan, Dec. 2020, pp. 1–6.

[39] L. Yang, F. Meng, Q. Wu, D. B. da Costa, and M.-S. Alouini, "Accurate closed-form approximations to channel distributions of RIS-aided wireless systems," *IEEE Wireless Commun. Lett.*, vol. 9, no. 11, pp. 1985–1989, Nov. 2020.

[40] K. Odeyemi, P. Owolawi, and O. Olakanmi, "Reconfigurable intelligent surface in wireless-powered interference-limited communication networks," *Symmetry*, vol. 13, no. 6, May 2021.

[41] M.-A. Badiu and J. P. Coon, "Communication through a large reflecting surface with phase errors," *IEEE Wireless Commun. Lett.*, vol. 9, no. 2, pp. 184–188, Feb. 2020.

[42] A. M. Salhab and M. H. Samuh, "Accurate performance analysis of reconfigurable intelligent surfaces over Rician fading channels," *IEEE Wireless Commun. Lett.*, vol. 10, no. 5, pp. 1051–1055, May 2021.

[43] Q. Tao, J. Wang, and C. Zhong, "Performance analysis of intelligent reflecting surface aided communication systems," *IEEE Commun. Lett.*, vol. 24, no. 11, pp. 2464–2468, Nov. 2020.

[44] I. Singh, P. J. Smith, and P. A. Dmochowski, "Optimal SNR analysis for single-user RIS systems in Ricean and Rayleigh environments," *IEEE Trans. Wireless Commun.*, vol. 21, no. 11, pp. 9834–9849, Nov. 2022.

[45] O. Waqar, "Performance analysis for IRS-aided communication systems with composite fading/shadowing direct link and discrete phase shifts," *Trans. Emerg. Telecommun. Technol.*, vol. 32, no. 10, p. e4320, Jun. 2021.

[46] A.-A. A. Boulogeorgos, A. Alexiou, and M. Di Renzo, "Throughput analysis of RIS-assisted UAV wireless systems under disorientation and misalignment," in *Proc. IEEE Global Commun. Conf. (GLOBECOM)*, Rio de Janeiro, Brazil, Dec. 2022, pp. 4485–4491.

[47] Z. Zhakipov, K. M. Rabie, X. Li, and G. Nauryzbayev, "Accurate approximation to channel distributions of cascaded RIS-aided systems with phase errors over Nakagami-m channels," *IEEE Wireless Commun. Lett.*, vol. 12, no. 5, pp. 922–926, May 2023.

[48] D. Tyrovolas, S. A. Tegos, E. C. Dimitriadou-Panidou, P. D. Diamantoulakis, C. K. Liaskos, and G. K. Karagiannidis, "Performance analysis of cascaded reconfigurable intelligent surface networks," *IEEE Wireless Commun. Lett.*, vol. 11, no. 9, pp. 1855–1859, Sep. 2022.

[49] R. C. Ferreira, M. S. P. Facina, F. A. P. De Figueiredo, G. Fraidenraich, and E. R. De Lima, "Bit error probability for large intelligent surfaces under double-Nakagami fading channels," *IEEE Open J. Commun. Soc.*, vol. 1, pp. 750–759, May 2020.

[50] S. A. Tegos, D. Tyrovolas, P. D. Diamantoulakis, C. K. Liaskos, and G. K. Karagiannidis, "On the distribution of the sum of double-Nakagami-m random vectors and application in randomly reconfigurable surfaces," *IEEE Trans. Veh. Technol.*, vol. 71, no. 7, pp. 7297–7307, Jul. 2022.

[51] T. Wang, G. Chen, and J. P. Coon, "Performance analysis of RIS-assisted full-duplex communication over correlated Nakagami-m fading channel," *IEEE Trans. Veh. Technol.*, early access, Oct. 10, 2023, doi: 10.1109/TVT.2023.3323277.

[52] N. A. Kamaruddin, A. Mahmud, M. Y. B. Alias, A. Abd Aziz, and S. Yaakob, "Performance evaluation of reconfigurable intelligent surface against distributed antenna system at the cell edge," *Electronics*, vol. 11, no. 15, Jul. 2022.

[53] T. Ahmed, A. S. M. Badrudduza, S. M. R. Islam, S. H. Islam, M. Ibrahim, M. Abdullah-Al-Wadud, and I. S. Ansari, "Enhancing physical layer secrecy performance for RIS-assisted RF-FSO mixed wireless system," *IEEE Access*, vol. 11, pp. 127 737–127 753, Nov. 2023.

[54] K. Singh, F. Karim, S. K. Singh, P. K. Sharma, S. Mumtaz, and M. F. Flanagan, "Performance analysis of RIS-assisted full-duplex communications with infinite and finite blocklength codes," *IEEE Trans. Commun.*, vol. 71, no. 7, pp. 4262–4282, Jul. 2023.

[55] V.-D. Phan, B. C. Nguyen, T. M. Hoang, T. N. Nguyen, P. T. Tran, B. V. Minh, and M. Voznak, "Performance of cooperative communication system with multiple reconfigurable intelligent surfaces over Nakagami-m fading channels," *IEEE Access*, vol. 10, pp. 9806–9816, Jan. 2022.

[56] T. Wang, G. Chen, M.-A. Badiu, and J. P. Coon, "Performance analysis of RIS-assisted large-scale wireless networks using stochastic geometry," *IEEE Trans. Wireless Commun.*, vol. 22, no. 11, pp. 7438–7451, Mar. 2023.

[57] Y. Ni, H. Zhao, Y. Liu, J. Wang, G. Gui, and H. Zhang, "Analysis of RIS-aided communications over Nakagami-m fading channels," *IEEE Trans. Veh. Technol.*, vol. 72, no. 7, pp. 8709–8721, Jul. 2023.

[58] N. Agrawal, A. Bansal, K. Singh, and C.-P. Li, "Performance evaluation of RIS-assisted UAV-enabled vehicular communication system with multiple non-identical interferers," *IEEE Trans. Intell. Transp. Syst.*, vol. 23, no. 7, pp. 9883–9894, Jul. 2022.

[59] T. N. Do, G. Kaddoum, T. L. Nguyen, D. B. da Costa, and Z. J. Haas, "Multi-RIS-aided wireless systems: Statistical characterization and performance analysis," *IEEE Trans. Commun.*, vol. 69, no. 12, pp. 8641–8658, Dec. 2021.

[60] H. Ibrahim, H. Tabassum, and U. T. Nguyen, "Exact coverage analysis of intelligent reflecting surfaces with Nakagami-M channels," *IEEE Trans. Veh. Technol.*, vol. 70, no. 1, pp. 1072–1076, Jan. 2021.

[61] D. Selimis, K. P. Peppas, G. C. Alexandropoulos, and F. I. Lazarakis, "On the performance analysis of RIS-empowered communications over Nakagami-m fading," *IEEE Commun. Lett.*, vol. 25, no. 7, pp. 2191–2195, Jul. 2021.

[62] S. Li, S. Yan, L. Bariah, S. Muhaidat, and A. Wang, "IRS-assisted full duplex systems over Rician and Nakagami fading channels," *IEEE Open J. Veh. Technol.*, vol. 4, pp. 217–229, Jan. 2023.

[63] I. Trigui, W. Ajib, W.-P. Zhu, and M. D. Renzo, "Performance evaluation and diversity analysis of RIS-assisted communications over generalized fading channels in the presence of phase noise," *IEEE Open J. Commun. Soc.*, vol. 3, pp. 593–607, Mar. 2022.

[64] V. K. Chapala, A. Malik, and S. M. Zafaruddin, "RIS-assisted vehicular network with direct transmission over double-generalized Gamma fading channels," in *Proc. IEEE 95th Veh. Technol. Conf. (VTC)*, Helsinki, Finland, Jun. 2022, pp. 1–6.

[65] M. A. Alves, G. Fraidenraich, R. C. Ferreira, F. A. P. De Figueiredo, and E. R. De Lima, "Multiple-antenna Weibull-fading wireless communications enhanced by reconfigurable intelligent surfaces," *IEEE Access*, vol. 11, pp. 107 218–107 236, Aug. 2023.

[66] A. Sikri, A. Mathur, and G. Kaddoum, "Joint impact of phase error, transceiver hardware impairments, and mobile interferers on RIS-aided wireless system over κ-μ fading channels," *IEEE Commun. Lett.*, vol. 26, no. 10, pp. 2312–2316, Oct. 2022.

[67] A. Al-Rimawi and A. Al-Dweik, "On the performance of RIS-assisted communications with direct link over κ-μ shadowed fading," *IEEE Open J. Commun. Soc.*, vol. 3, pp. 2314–2328, Nov. 2022.

[68] M. Charishma, A. Subhash, S. Shekhar, and S. Kalyani, "Outage probability expressions for an IRS-assisted system with and without source-destination link for the case of quantized phase shifts in κ-μ fading," *IEEE Trans. Commun.*, vol. 70, no. 1, pp. 101–117, Jan. 2022.

[69] G. R. d. L. Tejerina, C. R. N. da Silva, R. A. A. de Souza, and M. D. Yacoub, "On the extended η-μ model: New results and applications to IRS-aided systems," *IEEE Trans. Veh. Technol.*, vol. 72, no. 4, pp. 4133–4142, Apr. 2023.

[70] M. Abramowitz and I. A. Stegun, *Handbook of Mathematical Functions with Formulas, Graphs, and Mathematical Tables*, 10th ed. Washington, DC: US Dept. of Commerce: National Bureau of Standards, 1972.

[71] F. W. J. Olver, D. W. Lozier, R. F. Boisvert, and C. W. Clark, *NIST Handbook of Mathematical Functions*, 1st ed. Washington, DC: US Dept. of Commerce: National Institute of Standards and Technology (NIST), 2010.

[72] I. S. Gradshteyn and I. M. Ryzhik, *Table of Integrals, Series, and Products*, 7th ed. New York: Academic, 2007.

[73] Wolfram Research, Inc., *Wolfram Research*, Accessed: Dec. 12, 2023. [Online]. Available: http://functions.wolfram.com

[74] G. K. Karagiannidis, N. C. Sagias, and P. T. Mathiopoulos, "$N*$Nakagami: A novel stochastic model for cascaded fading channels," *IEEE Trans. Commun.*, vol. 55, no. 8, pp. 1453–1458, Aug. 2007.

[75] G. Fubini, "Sugli integrali multipli." *Rom. Acc. L. Rend. (5)*, vol. 16, no. 1, pp. 608–614, 1907.

[76] E. Kreyszig, *Advanced Engineering Mathematics*, 10th ed. New Jersey: John Wiley & Sons, 2010.

[77] M. M. Molu, P. Xiao, M. Khalily, L. Zhang, and R. Tafazolli, "A novel equivalent definition of modified Bessel functions for performance analysis of multi-hop wireless communication systems," *IEEE Access*, vol. 5, pp. 7594–7605, May 2017.

[78] F. D. A. García, F. R. A. Parente, M. D. Yacoub, and J. C. S. Santos Filho, "Exact κ-μ sum statistics," *IEEE Wireless Commun. Lett.*, vol. 12, no. 7, pp. 1284–1288, Jul. 2023.

[79] J. L. Schiff, *The Laplace Transform: Theory and Applications*, 1st ed. New York: Springer, 1999.

[80] D. Jackson, "A proof of Weierstrass's theorem," *Amer. Math. Monthly*, vol. 41, p. 309–312, 1934.

[81] E. Neuman, "Inequalities and bounds for the incomplete gamma function," *Results. Math.*, vol. 63, pp. 1209–1214, Jun. 2012.